Fluorescence-based sensing of the bioenergetic and physicochemical status of the cell

Mantovanelli, Luca; Gaastra, Bauke F.; Poolman, Bert

Published in:
Current Topics in Membranes

DOI:
10.1016/bs.ctm.2021.10.002

Publication date:
2021

CHAPTER ONE

Fluorescence-based sensing of the bioenergetic and physicochemical status of the cell

Luca Mantovanelli, Bauke F. Gaastra, and Bert Poolman*
Department of Biochemistry, University of Groningen, Groningen, the Netherlands
*Corresponding author: e-mail address: b.poolman@rug.nl

Contents

Current Topics in Membranes, Volume 88
ISSN 1063-5823
https://doi.org/10.1016/bs.ctm.2021.10.002

Abstract

Fluorescence-based sensors play a fundamental role in biological research. These sensors can be based on fluorescent proteins, fluorescent probes or they can be hybrid systems. The availability of a very large dataset of fluorescent molecules, both genetically encoded and synthetically produced, together with the structural insights on many sensing domains, allowed to rationally design a high variety of sensors, capable of monitoring both molecular and global changes in living cells or in *in vitro* systems. The advancements in the fluorescence-imaging field helped researchers to obtain a deeper understanding of how and where specific changes occur in a cell or *in vitro* by combining the readout of the fluorescent sensors with the spatial information provided by fluorescent microscopy techniques. In this review we give an overview of the state of the art in the field of fluorescent biosensors and fluorescence imaging techniques, and eventually guide the reader through the choice of the best combination of fluorescent tools and techniques to answer specific biological questions. We particularly focus on sensors for probing the bioenergetics and physicochemical status of the cell.

Abbreviations

cpFP	circularly permuted fluorescent protein
CTPE	chemogenetic tags with probe exchange
FAST	fluorescence-activating and absorption shifting tag
FLIM	fluorescence lifetime imaging
FP	fluorescent protein
FRAP	fast recovery after photobleaching
FRET	Förster resonance energy transfer
HILO	highly inclined and laminated optical sheet
PAFP	photoactivable fluorescent protein
PALM	photo-activated localization microscopy
POI	protein of interest
PSFP	photoswitchable fluorescent protein
SBP	substrate-binding protein
SMDM	single molecule displacement mapping
STORM	stochastic optical reconstruction microscopy
TICT	twisted intramolecular charge transfer
TCSPC	time correlated single photon counting
TIRF	total internal reflection fluorescence

1. Introduction

Fluorescence-based sensors can be divided into three groups: Fluorescent protein-based sensors, chemical probes and hybrid systems. Fluorescent proteins (FPs) have been known in the life sciences for several

decades (Shimomura, Johnson, & Saiga, 1962). Since the cloning of the *Aequorea victoria* gene for Green Fluorescent Protein (GFP) in 1992 (Prasher, Eckenrode, Ward, Prendergast, & Cormier, 1992), and its subsequent use as an *in vivo* fluorescent tag in 1994 (Chalfie, Tu, Euskirchen, Ward, & Prasher, 1994), FPs have been extensively used to obtain a deeper understanding of the structures and biochemical processes of living organisms. Compared to, *e.g.*, electron microscopy (EM) techniques, it now became possible to track macromolecules and structures in living cells and tissues, albeit with lower resolution than in EM. The imaging potential of GFP sparked the interest of many scientists and led to the discovery of new FPs with diverse and improved photophysical properties (Chudakov, Matz, Lukyanov, & Lukyanov, 2010; Rodriguez et al., 2017; Shinoda et al., 2018; Zhang, Gurtu, & Kain, 1996), allowing to gain a better understanding of the mechanism of action (Tsien, 1998) of fluorescent proteins. A color palette of FPs ranging from near ultra-violet (Tomosugi et al., 2009) to far-red (Kamper, Ta, Jensen, Hell, & Jakobs, 2018) is now available (*vide infra*).

By specifically labeling proteins of interest, it became possible to localize and determine the dynamics of macromolecules (Chamberlain & Hahn, 2000; Day & Schaufele, 2008), to discover protein interaction partners, and to perform protein turnover analyses (Knop & Edgar, n.d.; Trauth et al., 2020). FPs have been engineered to obtain pH-insensitive (Roberts et al., 2016; Shinoda et al., 2018) and highly monomeric (Campbell et al., 2020; Shaner et al., 2013) variants. Subsequently, FPs have been used to develop a great variety of sensors (Berg, Hung, & Yellen, 2009; Miyawaki et al., 1997; Nadler, Morgan, Flamholz, Kortright, & Savage, 2016) to study both molecular and global changes in the tagged macromolecule or structure of the cell. The availability of FPs emitting at different wavelengths allowed the application of the Förster Resonance Energy Transfer (FRET) mechanism to create sensors (Calamera et al., 2019; Miyawaki et al., 1997; Otten et al., 2019; Sadoine, Reger, Wong, & Frommer, 2021) and to determine interaction between proteins or protein domains (Ivanusic, Eschricht, & Denner, 2014; Kaufmann et al., 2020). Circularly permuted fluorescent proteins (cpFPs) variants (Topell, Hennecke, & Glockshuber, 1999) have been developed to create sensors (Kostyuk, Demidovich, Kotova, Belousov, & Bilan, 2019) to detect variations in the concentration of specific molecules. Finally, the development of photoactivatable (Lippincott-Schwartz & Patterson, 2009; Lukyanov, Chudakov, Lukyanov, & Verkhusha, 2005; Wang, Moffitt, Dempsey, Xie, & Zhuang, 2014) and photoswitchable

(Brakemann et al., 2011; Wazawa et al., 2021; Zhou & Lin, 2013) FPs, coupled with technological advancement in the microscopy field, allowed performing experiments beyond the diffraction limit of light, and a resolution of 20–30 nm has been obtained with optical microscopy (Shcherbakova, Sengupta, Lippincott-Schwartz, & Verkhusha, 2014). In recent years, technological advancements allowed to push the boundaries of what can be observed via optical microscopy even further: the recently developed system MINFLUX allows to localize single molecules in living cells with a resolution of less than 2 nm (Balzarotti et al., 2017).

Organic fluorescent dyes can be used for imaging purposes (Strack, 2021) or as biosensors (Fu & Finney, 2018), but the tagging of specific macromolecules is more challenging than with genetically encoded probes. However, in recent years several approaches for specific labeling of proteins inside cells have been developed (Cole, 2013; Takaoka, Ojida, & Hamachi, 2013). Chemical probes are typically characterized by more narrow excitation and emission spectra than FPs. Moreover, chemical probes generally are much more photostable and emit at least an order of magnitude more photons than FPs. A wide range of chemical probes varying in their photochemical and physical properties is available (Alexa Fluor, 2021; BODIPY, 2021), allowing to construct different type of sensors (Barreto-Chang & Dolmetsch, 2009; Liu et al., 2020). Another use of fluorescent dyes is in combination with other macromolecules. These dyes can be directly conjugated with specific sensing domains to create hybrid biosensors (Hu et al., 2014), or to antibodies for imaging purposes (Mao & Mullins, 2010). An additional way of using fluorescent dyes in combination with macromolecules is by using probes capable of interacting with specific binding pockets. These dyes need to be virtually non-fluorescent when unbound, and increase their fluorescence and change their lifetime upon interaction with the macromolecular partner. This system has been applied to create both hybrid protein-dye systems (Iyer et al., 2021; Plamont et al., 2016), and RNA-dye systems (Autour et al., 2018; Pothoulakis, Ceroni, Reeve, & Ellis, 2014), which can be used for imaging purposes (Gautier et al., 2008; Ouellet, 2016) or to develop biosensors (Jepsen et al., 2018; Tebo et al., 2018; Wang, Wilson, & Hammond, 2016).

The goal of this review is to give an overview of the available systems and to highlight their strengths and their weaknesses. We will describe the major uses of fluorescent tools in biological research and we will describe examples of sensors to track molecular and global changes both in solution and in living cells. Finally, given the extreme variety of available sensors and

techniques, we will provide the reader with a concept map to help choosing the best fluorescent tool and the best technique for analyzing the bioenergetics and physicochemical status of cells. We will focus on critical cellular parameters such as ATP (and other nucleotides), ionic strength, macromolecular crowding (excluded volume), membrane potential, NAD(P) and NAD(P)H levels, pH, temperature, viscosity and volume.

2. Currently available fluorescent molecules

The fluorescence molecules currently used in biological research can be divided into two categories: genetically encoded fluorescence proteins (Zhang et al., 1996) and fluorogenic molecules. The latter can be further distinguished into two subcategories: molecules that do not require a binding partner to emit detectable fluorescence upon excitation (Strack, 2021), and molecules that greatly increase their emission intensity after binding to a target molecule (Iyer et al., 2021; Plamont et al., 2016). Both fluorescent proteins and fluorogenic molecules have advantages and disadvantages, and they greatly differ in their mechanism of action.

2.1 Fluorescent proteins

2.1.1 Chromophore formation in fluorescent proteins

The structural studies performed on GFP (Yang, Moss, & Phillips, 1996), and subsequently on other FPs (Marshall, 2000; Park, Kang, & Yoon, 2016; Wachter, Elsliger, Kallio, Hanson, & Remington, 1998), unveiled the mechanisms through which these proteins gain fluorescence. All FPs have a β-barrel structure with an embedded α-helix (Fig. 1A) (Yang et al., 1996). The three amino acids located on this helix, which in wild type GFP are Ser65, Tyr66 and Gly67, undergo a post-translational self-modification that yields the chromophore. The proposed mechanism of formation of the GFP chromophore (Heim, Prasher, & Tsien, 1994) consists of a cyclization-dehydration-oxidation sequence (Fig. 1B). Briefly, the nucleophilic attack of the amino group of Gly67 onto the carbonyl group of Ser65 results in the formation of the imidazolidinone ring with elimination of water. Subsequently, the oxidation of the C^{α}-C^{β} bond of Tyr66 causes the formation of a large π system of which the electrons can be excited with photons of proper wavelength (Reid & Flynn, 1997). The radiative decay of the electrons to the ground energy level is responsible for the emission of light. Other FPs undergo different post-translational modification and there is variation in the three consecutive amino acids, but the first step

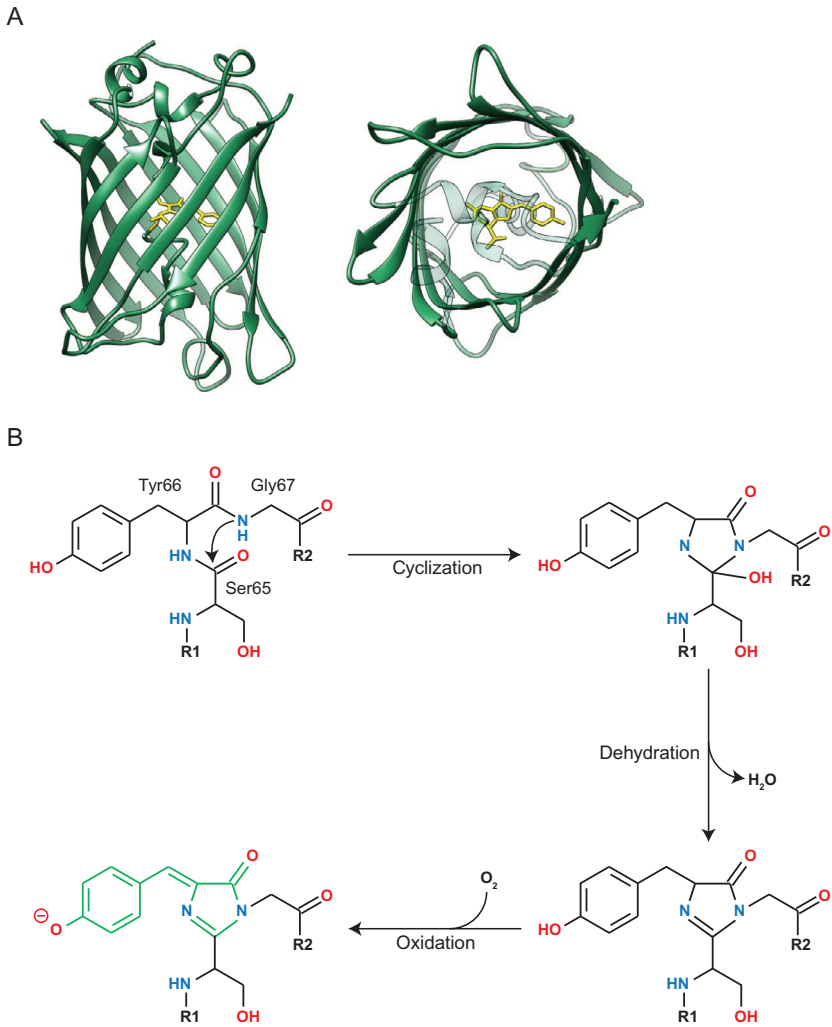

Fig. 1 (A) Structure of wild type GFP obtained via UCSF Chimera (Pettersen et al., 2004). Structure used for the representation: 1EMA. (B) Three step mechanism for the chromophore formation. Only the negatively charged phenolate is fluorescent. The uncharged protonated phenol group is not fluorescent. Scheme based on the work by Barondeau, Putnam, Kassmann, Tainer, and Getzoff (2003).

for all FPs is represented by the cyclization of the first and third residue that form the chromophore (residues 65 and 67 in wild type GFP). The chromophore of some red FPs develops directly from GFP-like chromophores, with a further oxidation step commonly referred to as oxidative redding

pathway (Verkhusha, Chudakov, Gurskaya, Lukyanov, & Lukyanov, 2004; Wachter, Watkins, & Kim, 2010). In other cases, the red chromophore develops from GFP-like chromophores that are excited by a laser pulse in the ultraviolet range, generating the so-called photoconvertible FPs (Ando, Hama, Yamamoto-Hino, Mizuno, & Miyawaki, 2002; Mizuno et al., 2003). Finally, another proposed mechanism of formation of red chromophores is via the formation of blue emitting chromophore intermediates, which undergo a further oxidation step to generate the red emitting molecule (Pletnev, Subach, Dauter, Wlodawer, & Verkhusha, 2010; Strack, Strongin, Mets, Glick, & Keenan, 2010). An extensive overview of chromophore formation is provided by Stepanenko et al. (2011).

For many years it was believed that Gly67 in GFP and other FPs was essential for the formation of the chromophore (Barondeau, Kassmann, Tainer, & Getzoff, 2005; Sniegowski, Phail, & Wachter, 2005). However, a recent study described the first functional FP containing a G67A mutation (Roldán-Salgado, Sánchez-Barreto, & Gaytán, 2016). Nevertheless, both residues 66 and 67 are highly conserved within all FPs, and all naturally occurring GFP-like proteins are characterized by the presence of Tyr66 (Heim et al., 1994). Mutations of residue 66 are less rare, and in fact Tyr66 can be substituted with any aromatic amino acid, resulting in chromophores that have a blue-shifted emission compared to GFP (Heim et al., 1994). Amino acids at position 65 can be diverse among FPs, yielding chemically distinct chromophores and proteins that emit light at different wavelengths. Although residues 65–67 are crucial for chromophore formation, they are not the only players responsible for the photochemical characteristics of FPs. A Tyrosine in position 203, for example, has a key role in the formation of yellow emitting chromophores due to a π-stacking interaction between the aromatic ring of Tyr203 and the chromophore (Wachter et al., 1998). Residues Glu222 and His203 are crucial for the formation of photoactivatable FPs (Henderson et al., 2009), and in general amino acidic modifications both in the chromophore and in the β-barrel can lead to chromophores with different emission wavelength, quantum yield and brightness (Box 1). For a comprehensive overview of amino acidic substitutions in FPs that lead to different chromophores we refer to the review by Stepanenko et al (Stepanenko et al., 2011). Further modifications in the structure of FPs have been deployed to modify other physical-chemical parameters, such as pH sensitiveness (Shinoda et al., 2018) or tendency to dimerize (Shaner et al., 2013) (among others). More recently, modifications that rearrange the structure of FPs by

BOX 1 Fluorescence-related terms

Fluorescent quantum yield

The quantum yield of a fluorescent molecule represents the ratio between the number of photon emitted by a molecule and the number of photons absorbed.

Brightness

The brightness of a fluorescent molecule indicates the sensitivity and the signal-to-noise ratio for the detection. It is a value given by the Fluorescent Quantum Yield multiplied by the molar extinction coefficient. Since the molar extinction coefficient depends on the wavelength, the brightness will depend on the chosen excitation wavelength.

Quenching

Quenching is used to describe processes that decrease the fluorescence of a fluorescent molecule. It can depend on different factors: in a FRET pair the acceptor acts as a dynamic quencher for the donor, static quenching can occur when a fluorescent molecule aggregates, and a dark quencher can absorb the fluorescence of a fluorescent molecule and dissipate it as heat.

Photobleaching

Photobleaching occurs when a fluorescent molecule is photochemically altered. This can happen due to the cleavage of covalent bonds or due to reactions between the fluorophore and other molecules. The cleavage of covalent bonds can occur in the transition of the fluorophore from a singlet to the triplet state. Such transition is formally forbidden, and the probability of occurring differs for various fluorescence molecules: some molecules photobleach after absorbing a few photons, while other molecules can undergo several absorption and emission cycles before being destroyed.

generating circularly permuted FPs (cpFPs) (Kostyuk et al., 2019) and split FPs (Romei & Boxer, 2019) have been successfully deployed to develop sensors with specific (ligand-binding) properties.

2.1.2 Maturation of fluorescent proteins

Once a FP is expressed, it needs to go through several stages in a process called maturation to become functional as fluorophore (Remington, 2006). The first step involves the folding of the protein, and here the FP assumes its characteristic β-barrel conformation. Next, the three key amino acids that form the chromophore need to undergo the processes of cyclization, dehydration and oxidation (Fig. 1B). The protein folding is relatively fast and normally takes less than a minute (Naganathan & Muñoz, 2005).

On the other hand, the full formation of the chromophore can be very slow, with the final oxidation step being rate-limiting (Ma, Sun, & Smith, 2017). Maturation of FPs depends on different factors: the amino acidic sequence of the protein, which can be modified to obtain faster maturing FPs (Balleza, Kim, & Cluzel, 2018); the environment (host) in which the protein is expressed, which influences both the speed of protein folding and chromophore formation (Hebisch, Knebel, Landsberg, Frey, & Leisner, 2013); the temperature at which the organism expressing the protein is grown (Guo, Xu, & Gruebele, 2012); and the presence of oxygen in the environment (the β-barrel type fluorophore will not be able to mature in the absence of oxygen; Ma et al., 2017). Overall the maturation process can last from 5 minutes for optimized FPs, such as super-folder GFP expressed in *Escherichia coli* under optimal conditions (Pédelacq, Cabantous, Tran, Terwilliger, & Waldo, 2006), up to more than 1 hour (Balleza et al., 2018), depending on the aforementioned factors.

2.1.3 The effect of pH on fluorescent proteins

Most FPs are sensitive to changes in the environmental pH. Wild-type GFP fluorescence is stable in the pH range from 6 to 10, but the fluorescence decreases below pH 6 and increases at pH values higher than 10 (Campbell, 2001). Other GFP variants display greater pH sensitivity (Mahon, 2011). The effect of pH on FPs has been exploited to obtain FPs highly sensitive to pH changes, which have subsequently been employed as pH sensors (Kollenda et al., 2020; Liu et al., 2021; Mahon, 2011; Shen, Rosendale, Campbell, & Perrais, 2014). In parallel, FPs insensitive to pH in the physiological range (pH 6–8) have been developed (Roberts et al., 2016; Shinoda et al., 2018). A decrease in fluorescence stability at lower pH values has been observed in all β-barrel type fluorescent proteins, leading to the hypothesis that the protonated form of the chromophore has lost the ability to emit fluorescence (Haupts, Maiti, Schwille, & Webb, 1998; Ward, Prentice, Roth, Cody, & Reeves, 1982). Studies on denatured wild-type GFP showed that the chromophore has pH-dependent excitation and emission spectra due to the ionization of the phenolic group of Tyr66 (Campbell, 2001), with the phenolate form of the chromophore being responsible for the observed fluorescence. The pK_a for the transition from uncharged phenol to phenolate is 8.1 (Campbell, 2001). With such a high pK_a it is surprising that the stability of wild type GFP is maintained until pH 6. However, it is important to remember that the chromophore in non-denatured FPs is buried inside the β-barrel structure, which shields it

from the external environment (Ward et al., 1982). Environmental pH changes need to first alter and partially denature the structure of the mature FP in order for protons to be able to interact with the chromophore and convert it from the anionic to the neutral form.

2.1.4 Photoactivatable and photoswitchable fluorescent proteins

In recent years the use of photoactivatable and photoswitchable FPs (PAFPs and PSFPs respectively) has grown, following the development of super-resolution imaging techniques (Nienhaus & Nienhaus, 2017). The use of PAFPs and PSFPs allow for the conversion of FPs from a dark form to a bright form or, *e.g.*, a green to red conversion by altering the hydrogen bonding and extending the conjugated double bond network of the fluorophore (Lukyanov et al., 2005). Briefly, PAFPs and PSFPs excited at a first specific wavelength fluoresce at a lower wavelength before being activated, or do not fluoresce at all. Activation occurs upon excitation with a laser pulse at a specific wavelength, typically 405 nm (Wang et al., 2014). By properly tuning the power and the duration of the laser pulse it is possible to activate only few molecules from the population of PAFPs and PSFPs, which can then be excited with the desired, specific wavelength and imaged. PSFPs can be reconverted to their dark state by exciting them with a third specific wavelength laser pulse (Zhou & Lin, 2013). The mechanism through which these proteins can gain fluorescence and switch from a dark to a bright state is via a *cis-trans* isomerization of the chromophore, which is triggered by the applied laser pulse. For a more detailed analysis of the mechanisms of photo-activation and photoswitching of PAFPs and PSFPs we redirect the reader to the review by Lukyanov et al. (2005) and by Zhou and Lin (2013).

2.1.5 Comparison of fluorescent proteins

In the last thirty years many different FPs have been developed, with different emission wavelength (Fig. 2), brightness, quantum yield, maturation time and pH sensitivity. We report in Table 1 an overview of the most commonly used FPs and related information (when available) about their chemical and photophysical properties.

2.2 Fluorogenic molecules

Fluorogenic molecules have been used extensively in biological research (Braut-Boucher et al., 1995; Gray, Mitchell, & Searles, 2015; Liu et al., 2020). Some of the main advantages of these molecules over FPs are that

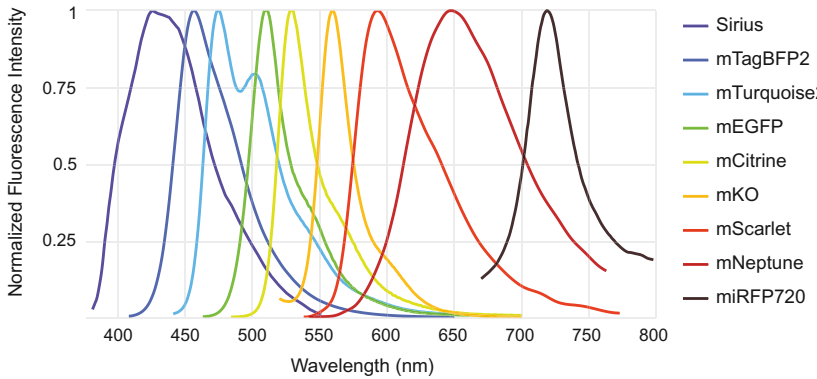

Fig. 2 Normalized Emission spectra of selected proteins from Table 1.

Table 1 List of some common fluorescent proteins with emission spectra ranging from dark blue to near infra-red.

Name	Ex max (nm)	Em max (nm)	Quantum Yield	Brightness	pKa	FPbase ID
Sirius*	355	424	0.24	3.6	3.0	BU5R3
EBFP2	383	448	0.56	17.9	5.3	DVMQ7
mTagBFP2*	399	454	0.64	32.3	2.7	ZO7NN
mTurquoise2*	434	474	0.93	27.9	3.1	7AV5G
mCerulean3	433	475	0.87	34.8	3.2	TWJXO
TagCFP	458	480	0.57	21.1	4.7	WRK8K
mEGFP*	488	507	0.60	33.6	6.0	QKFJN
mNeonGreen	506	517	0.80	92.8	5.7	ZRKRV
Gamillus	504	519	0.90	74.7	3.4	21PQ5
mVenus	515	527	0.64	66.6	5.5	WCSN6
mEYFP	515	528	0.62	49.0	6.9	SBLM5
mCitrine*	516	529	0.74	69.6	5.7	3Q37R
mKO*	548	559	0.60	31.0	5.0	RR1M4
mOrange2	548	562	0.69	49.0	6.5	5GR1V
mTangerine	568	585	0.30	11.4	5.7	N63O3
mScarlet*	569	594	0.70	70.0	5.3	FVS3D
mCherry	587	610	0.22	15.8	4.5	ZERB6
mNeptune*	600	650	0.20	13.4	5.4	1LT8G
miRFP	674	703	0.10	9.0	4.3	HO9GG
SNIFP	697	720	0.02	3.3	4.5	Q5F5J
miRFP720*	702	720	0.06	6.0	4.5	AJLWS
Photoswitchable Fluoresent Proteins						
mMaple3 (Green)	491	506	0.37	5.8	-	MNH1D
mEos3.2 (Green)	507	516	0.84	53.3	5.4	VUXRF
mEos3.2 (Red)	572	580	0.55	17.7	5.8	VUXRF
mMaple3 (Red)	568	583	0.52	12.5	-	MNH1D

The rows are color coded according to the emission wavelength of the fluorescent protein. Columns are, from left to right: Name of the fluorescent protein, Maximum Excitation wavelength, Maximum Emission wavelength, Fluorescent Quantum Yield, Brightness, pKa and FPbase ID. The normalized emission spectra of the proteins denoted with an asterisk (*) are visualized in Fig. 2.

they do not have to mature, have greater photostability, emit more photons and are much smaller. Some fluorogenic probes can be used as standalone molecules (Braut-Boucher et al., 1995; Liu et al., 2020) due to their natural high brightness and quantum yield, while others need to be paired with macromolecules (Iyer et al., 2021; Plamont et al., 2016; Pothoulakis et al., 2014), since only after interacting with a specific binding pocket they become (highly) fluorescent. Possible limitations of fluorogenic molecules, especially for *in vivo* research, are (i) their potential cytotoxicity and impact on the growth of cells, (ii) the non-trivial specific labeling of macromolecules or supramolecular structures and (iii) the targeting to specific compartments. Commonly employed fluorogenic molecules are the ATTO, Alexa Fluor and Cy-dye series with colors ranging from UV to infrared. The choice of the more appropriate dye depends on many factors, such as its photostability, brightness, quantum yield, lifetime, as well as its tendency to interact with different biological structures.

2.2.1 Organic dyes

Organic dyes as standalone molecules are available for different purposes. One of the main applications of these dyes is for cell imaging. For example, Calcein-AM and BCECF-AM (AM refers to acetoxymethyl ester form) are cell permeant dyes that are demethylated upon entering the cell and thereby trapped on the inside (Allen & Cleland, 1980). These dyes allow observing cell features that would not be as easy to distinguish with normal wide-field microscopy. BCECF and derivatives are commonly used to monitor the cytoplasmic pH of cells (Boens et al., 2006). Standalone dyes are also used to monitor physical chemical parameters of the environment in which they are present. For example, Calcein can be used to monitor volume changes (Gabba et al., 2020) due to its self-quenching (see Box 1) at high concentrations (Patel, Tscheka, & Heerklotz, 2009) or its quenching by proteins inside cells (Solenov, Watanabe, Manley, & Verkman, 2004), while molecular rotors such as BODIPY rotors can be used to monitor viscosity of solutions (bulk) or the local viscosity inside the cell (Liu et al., 2020). Molecular rotors can rotate one segment of their structure with respect to the rest of the molecule, causing a change in the ground-state and excited-state energy levels, which is reflected in a variation of the lifetime of the excited molecule. The amount of this energy change (and of lifetime variation) is dependent on the amount of intramolecular rotation, which depends on the environment (Liu et al., 2020).

Organic dyes also have a fundamental role in click chemistry. Here, a specific ligand conjugated with a dye can interact with its binding partner,

allowing for detection of particular targets. These reactions can be performed both *in vitro* and *in vivo*. In particular, it is possible to perform *in vitro* bioconjugation reactions of natural amino acids on a protein surface, specifically targeting exposed cysteine (Kim et al., 2008), lysine (Larda, Pichugin, & Prosser, 2015), tyrosine (Dorta, Deniaud, Mével, & Gouin, 2020) and tryptophan (Ladner, Turner, & Edwards, 2007) residues. Several *in vivo* techniques are available for labeling molecules, such as the SNAP-tag method, in which a protein of interest (POI) is functionalized with an enzyme tag that allows the covalent labeling of the protein (Cole, 2013), the incorporation of unnatural amino acids in the sequence of a POI (Laxman, Ansari, Gaus, & Goyette, 2021), allowing their direct chemical modification, and the Staudinger-Bertozzi ligation reaction (Saxon, Armstrong, & Bertozzi, 2000), which consists in the ligation of a triarylphosphine conjugate reporter to an azide-functionalized biomolecular analogue that can be incorporated in cell structures, allowing for the detection of many different macromolecules, such as glycans, lipids, DNA and proteins (van Berkel, van Eldijk, & van Hest, 2011).

Another use of non-interacting organic dyes is via conjugation with antibodies (Mao & Mullins, 2010); these binding partner molecules can then be used to target specific structures of the cell, allowing multicolor imaging (Westerhof, Li, Bachman, & Nelson, 2016). A caveat of these techniques is that cells need to be permeabilized in order for the antibodies to reach their targets, making it impossible to be used *in vivo*. Fluorogenic dyes can also be conjugated with peptides (Cummings et al., 2002), allowing for example the detection of enzymatic reactions capable of digesting the polypeptide sequence. The list of fluorogenic dyes and their application is very extensive, and for a more detailed review on the topic we redirect the reader to the extensive works of Specht, Braselmann, and Palmer (2017), Takaoka et al. (2013) and Agouridas et al. (2019).

2.2.2 Hybrid systems

The use of hybrid systems as fluorescent tools can be very advantageous as they combine the best of FPs (specific targeting) and organic dyes (photophysical properties) (Fig. 3C). As long as a specific binding pocket is present in the protein or RNA, the dyes will interact with the macromolecule and emit fluorescence. Many dyes with different chemical structures and capable of binding to different cellular components are available, allowing for detection and imaging of membranes (Spötl, Sarti, Dierich, & Möst, 1995), DNA (Dirks & Tanke, 2006) and RNA (Dirks & Tanke, 2006) among other structures. Recently, proteins with more or less specific dye

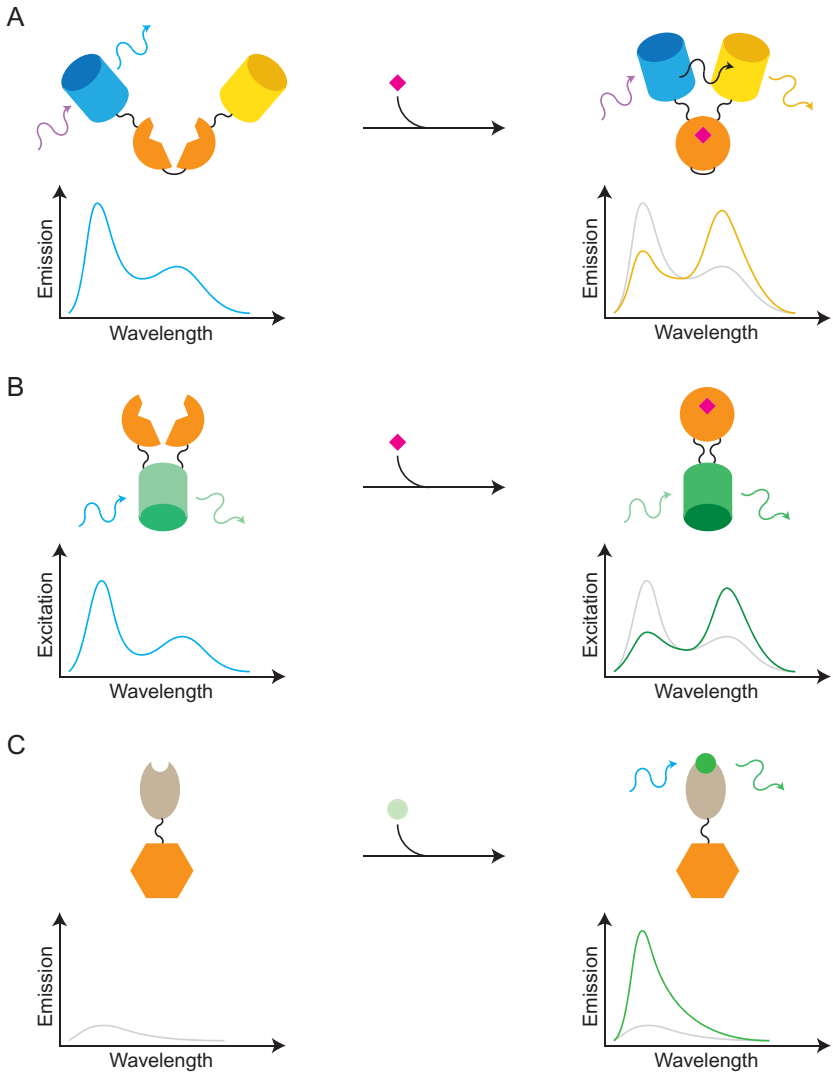

Fig. 3 Schematic of different types of sensors. (A) FRET sensor with a CFP as donor and a YFP as acceptor. Upon binding of the target molecule the two FPs are brought closer to each other with subsequent increased FRET, which can be detected in the emission spectrum as a decrease in intensity in the CFP peak or an increase in the YFP peak. (B) Ratiometric sensor based on a cpFP. After the binding of the POI with the substrate, the cpFP changes its conformation with a subsequent change in the excitation spectrum, where one of the peaks increases in intensity and the other decreases. (C) Hybrid system for labeling a POI. The POI is linked to a protein that can bind a fluorogenic dye. Before binding to its partner, the dye's brightness is very low. After the binding of the dye, the system increases its fluorescence emission.

binding motifs have been developed (Iyer et al., 2021; Plamont et al., 2016). These proteins can be used for genetic tagging of targets in the same way that FPs are used. The fluorescent dyes bind to these proteins, which leads to an instantaneous increase in fluorescence. These hybrid systems do not require protein maturation and labeling can be done in the absence of oxygen, allowing for studies in anaerobes (Iyer et al., 2021). Importantly, the reversible binding of organic fluorophores to these proteins and the superior photophysical properties of organic fluorophores enable long-term fluorescence microscopy of living cells. A caveat of this method compared to FPs is that the dyes need to be membrane permeable and they should not bind to other cell structures (Iyer et al., 2021). The hybrid systems, known as fluorescence-activating and absorption shifting tag (FAST) (Plamont et al., 2016) and Chemogenetic Tags with Probe Exchange (CTPEs) (Iyer et al., 2021), have been also used for multicolor imaging (Tebo et al., 2021) and subsequent development of FRET sensors.

Another recent innovation is the development of organic dyes and RNA aptamers capable of interacting with each other (Pothoulakis et al., 2014). Both green and red variants are available (Autour et al., 2018; Pothoulakis et al., 2014), which can be used concurrently, since different dyes interact with different aptamers. These systems provide a tool to image RNA in a way not achievable with other organic dyes or with the use of FPs (Zhang et al., 2015), allowing fast detection of the transcribed nucleic acid. These fluorescent systems have also been used to develop sensors, both in the form of single color sensors (Kellenberger, Chen, Whiteley, Portnoy, & Hammond, 2015) as well as FRET based (Jepsen et al., 2018), for detecting small molecules or other RNA sequences (Jepsen et al., 2018). An advantage of using RNA-type of sensors compared to protein-based sensors is that the detection time of the analytes is faster, since the RNA does not need to be translated and folded into a mature protein. RNA folding occurs during the transcription process, allowing for the fast formation of a binding pocket (Zhang et al., 2015). A major drawback in developing this kind of sensor, however, is that RNA prediction tools are much less advanced than the corresponding methods for proteins.

3. Labeling of (macro)molecules of interest

Tagging of molecules with fluorescent probes can be achieved in different ways, and below we briefly present the common strategies to label molecules and to selectively localize proteins, lipids and nucleic acids in

the cell. This overview is not comprehensive and only outline possible scenarios. More extensive overviews are provided by Specht et al. (2017) and by Dirks and Tanke (2006).

3.1 Protein labeling

Tagging of proteins with fluorescent reporters can serve as a tool to localize proteins within the cell and visualize particular cell structures and cell compartments (Chalfie et al., 1994). The most common way of tagging proteins with fluorescent reporters is through the creation of a fusion construct of the POI with a FP (Chalfie et al., 1994). Once the construct is translated, the fully matured FP will emit fluorescence upon excitation. In case of GFP and derivatives the fluorescent proteins adds a 27 kDa domain to the POI, and one needs to make sure that the localization of the POI is not affected by the tagging. If the POI needs to be localized immediately after translation, or if the conditions in which the POI needs to be expressed require absence of oxygen (such as in obligated anaerobes), the preferred imaging tool would be FAST (Plamont et al., 2016) or CTPE (Iyer et al., 2021), for which the fluorescence development is not dependent of oxygen and for which there is no delay between protein expression and fluorescence emission. Another way to visualize a POI is through the incorporation into proteins of fluorophores conjugated to unnatural amino acids (Laxman et al., 2021), but the number of dyes available for direct protein labeling is limited.

3.2 Membrane labeling

The use of membrane proteins coupled to fluorescent tags for imaging membranes can help understanding the functional dynamics and structure of this organelle (Costantini et al., 2015). This approach will not be discussed here as it essentially takes the route of protein labeling. Alternatively, one can visualize membranes by adding organic dyes capable of intercalating in the lipid bilayer (Collot, Boutant, Fam, Danglot, & Klymchenko, 2020). A drawback of using these dyes is in most cases the inability to specifically label a particular membrane. More advanced techniques such as *in vitro* conjugation of lipids with organic dyes and the application of a lipid binding domains have increased the specificity of membrane labeling (Kundu, Chandra, & Datta, 2021; Shi, Heegaard, Rasmussen, & Gilbert, 2004). For instance, the lactadherin C2 domain allows the detection of phosphatidylserine (PS) lipids, whereas other protein domains and antibodies (labeled with

fluorescent probes) have been used for phosphoinositides (PI) (Várnai & Balla, 2006; Wakelam, 2014). Biochemical detection techniques now allow quantification of all seven phosphoinositides, and the use of fluorescently tagged PI-binding domains enables real-time visualization of most of them in intact cells.

3.3 Nucleic acids labeling

One of the first ways of labeling nucleic acids was via staining of the DNA through the use of organic molecules capable of entering the cell and intercalating into the DNA double helix. This method, however, prohibited long-term *in vivo* studies (Salic & Mitchison, 2008), such as monitoring the structure and dynamics of DNA during the cell cycle, due to the damage done to the DNA by the staining molecule, but recently less damaging dyes have been developed (Qu et al., 2011). Another method for labeling nucleic acids is via the use of probes capable of entering the cell and binding specific sequences of DNA or RNA (Dirks & Tanke, 2006). Linear Phosphodiester Oligodeoxynucleotides (Politz, Taneja, & Singer, 1995), Peptide Nucleic Acids (Molenaar et al., 2003), 2′-O-methyl RNAs (Molenaar, Abdulle, Gena, Tanke, & Dirks, 2004) and Locked Nucleic Acids (Darfeuille, Hansen, Orum, Primo, & Toulmé, 2004) are a few examples of probes that can target specific nucleic acid sequences. These probes are made of molecules that pair either with DNA or RNA, and that are conjugated with a fluorescence reporter. After entering the cells, these probes cannot be metabolized, allowing to visualize nucleic acids for an extended period of time. Another way to label nucleic acids is via the use of labeled DNA or RNA binding proteins. Labeling of proteins can be accomplished with any of the methods reported in Section 3.1. A drawback of the method is that some DNA regions can be elusive and not have a protein-binding partner. An elegant solution to this problem could be the use of CRISPR-Cas with a labeled inactive Cas protein (Deng, Shi, Tjian, Lionnet, & Singer, 2015). The guide RNA used in the system would then allow labeling virtually any location on the DNA and any RNA sequence. Finally, a series of tools for RNA imaging developed in the past few years is represented by aptamers capable of binding organic dyes, which in turn can emit fluorescence (Pothoulakis et al., 2014). Several versions of these aptamers have been developed (Ouellet, 2016), allowing for labeling of virtually all types of RNA (Okuda, Fourmy, & Yoshizawa, 2017) and for multicolor imaging.

4. Sensors and methods of detection

There are different types of fluorescence-based sensors: ratiometric sensors, intensiometric sensors and sensors based on Förster Resonance Energy Transfer (FRET). In ratiometric sensors (Fig. 3B), the readout is a ratio of two wavelengths (usually two spectral maxima or a maximum and isosbestic point) in either the excitation or the emission spectrum. Ratiometric sensors have the benefit that the concentration of the fluorescent protein or probe does not have a direct influence on the readout. In intensiometric sensors, the signal is defined by the change in emission intensity upon stable excitation. Knowing the concentration of these sensors is critical for the analysis, which is often not possible due to cell-to-cell variations and changes in sensor concentration in the course of an experiment. Intensiometric sensors are in most cases disfavored when ratiometric or Forster Resonance Energy Transfer (FRET)-based approaches are available.

FRET involves the transfer of resonance energy from a donor fluorophore to an acceptor fluorophore without emission of light (Förster, 1948) (Fig. 3A). This energy transfer occurs when (i) the donor's emission has a higher energy (shorter wavelength) than the acceptor's emission (Shrestha, Jenei, Nagy, Vereb, & Szöllősi, 2015); (ii) the donor emission spectrum overlaps with the acceptor excitation spectrum (Shrestha et al., 2015); and (iii) the donor and the acceptor are at a distance between 3 and 7 nm from each other, depending on the donor-acceptor pair. The choice of donor and acceptor can be complex, as it is necessary to take into account many factors, such as the quantum yield and brightness of both fluorophores as well as the overlap of their spectra. An excellent review on FRET couples is provided by Bajar, Wang, Zhang, Lin, and Chu (2016). The apparent FRET efficiency can be calculated according to Eq. (1):

$$E_{app} = \frac{I_A}{I_A + I_D} \tag{1}$$

where I_A and I_D are the emission intensity of the acceptor and of the donor, respectively. A good overlap of the donor's emission and acceptor's excitation spectrum is necessary for a high efficiency of energy transfer, which is never 100%. That means that after exciting the donor and detecting the emission of the acceptor, the emission of the donor will also be detected.

According to Eq. (1), when the brightness and the quantum yield of the donor are high compared to the values for the acceptor, the apparent FRET will be low.

A more accurate way of obtaining the FRET efficiency is by measurement of the lifetime of the donor (Periasamy, Mazumder, Sun, Christopher, & Day, 2015). The lifetime of fluorescent molecules is described by the reciprocal of the sum of radiative and non-radiative decays (Eq. 2), and it is directly related to the quantum yield (Eq. 3):

$$\tau = \frac{1}{k_r + k_{nr}} \tag{2}$$

$$\Phi = \frac{k_r}{k_r + k_{nr}} \tag{3}$$

where τ is the lifetime, k_r is the rate of the radiative decay, k_{nr} is the rate of the non-radiative decays and Φ is the quantum yield. In the case of FRET, the rate of energy transfer must also be taken into consideration (Eqs. 4 and 5):

$$\tau_{DA} = \frac{1}{k_r + k_{nr} + k_{ET}} \tag{4}$$

$$\Phi_{DA} = \frac{k_r}{k_r + k_{nr} + k_{ET}} \tag{5}$$

where τ_{DA} is the lifetime of the donor in the presence of the acceptor, Φ_{DA} is the quantum yield of the donor in the presence of the acceptor and k_{ET} is the rate of energy transfer. The real FRET efficiency is then obtained from Eq. (6):

$$E = 1 - \frac{\tau_{DA}}{\tau_D} \tag{6}$$

where τ_D is the lifetime of the donor alone.

FRET can be used both *in vitro* and *in vivo*, such as for co-localization studies (Augustinack, Sanders, Tsai, & Hyman, 2002), conformational changes in macromolecules (Gauer et al., 2016) and molecule detection by sensors (Otten et al., 2019). The FRET efficiency can also be calculated as a function of the distance between the donor and the acceptor (Eq. 7):

$$E = \frac{R_0^6}{R_0^6 + r^6} \tag{7}$$

where R_0, the Förster distance, is the distance between donor and acceptor at which 50% FRET efficiency, and r is the actual distance between donor and acceptor.

The Förster distance depends on the overlap integral of the donor emission spectrum and the acceptor absorption spectrum, as well as on their reciprocal molecular orientation and the refractive index of the medium (Eq. 8):

$$R_0^6 = \frac{2.07}{128\,\pi^5\,N_A}\,\frac{\kappa^2 Q_D}{n^4}\int F_D(\lambda)\varepsilon_A(\lambda)\lambda^4 d\lambda \tag{8}$$

where Q_D is the quantum yield of the donor in the absence of the acceptor, κ (Prasher et al., 1992) is the dipole orientation factor, n is the refractive index of the medium, N_A is the Avogadro constant, F_D is the donor emission spectrum normalized to an area of 1, ε_A is the acceptor molar extinction coefficient, and λ is the wavelength. The value κ can vary from 0 to 4, and normally it is assumed to be 2/3 for freely rotating fluorescent pairs, which reflects the average of all the possible orientations that the two molecules can take (van der Meer, 2002). Fluorescent anisotropy measurements can be performed to ascertain that the donor and the acceptor are freely rotating (van der Meer, 2002).

4.1 Organic dyes as sensors

Standalone organic dyes can be used to sense physical chemical parameters in solutions (Bittermann, Grzelka, Woutersen, Brouwer, & Bonn, 2021), vesicles (McNamara & Rosenzweig, 1998) and cells (Oliveira et al., 2018). Dyes have been developed that detect changes in the concentration of small molecules like oxygen (Mirabello, Cortezon-Tamarit, & Pascu, 2018), ATP (Wang et al., 2016), reactive oxygen species (Choi, Yang, & Weisshaar, 2015), protons (pH) (Ozkan & Mutharasan, 2002), iron (Ma, Abbate, & Hider, 2015) and calcium (Paredes, Etzler, Watts, & Lechleiter, 2008) among others, and dyes that can detect global changes in solutions, such as molecular rotors used for measuring the viscosity of a solution (Liu et al., 2020), or self-quenching probes that report volume changes (Gabba et al., 2020).

4.2 Fluorescent protein-based sensors

The physical chemical properties of FPs have been exploited extensively to develop different types of sensors, and for an extensive review on single

fluorescent protein-based biosensors we redirect the reader to the review by Nasu et al (Nasu, Shen, Kramer, & Campbell, 2021). One of the best-documented properties of FPs is the pH dependent fluorescence. This property has been used to develop sensors that are highly sensitive to pH changes (Liu et al., 2021; Mahon, 2011), which have been used to determine the pH inside of living cells. Another use of FPs is their possible employment as viscosity sensors, as it has been observed that lifetime of some fluorescent proteins can change with the refractive index (Davidson et al., 2020) and that the time-resolved anisotropy is affected by the viscosity of the environment (Borst, Hink, van Hoek, & Visser, 2005; Suhling, Davis, & Phillips, 2002).

The development of circularly permuted FPs (cpFPs) provided researchers with tools for designing a whole new range of sensors (Kostyuk et al., 2019). In the structure of circularly permuted proteins the N- and the C-terminus are fused together with a linker. New N- and C-termini are created in another part of the protein, creating a gap in a portion that was originally continuous (Topell et al., 1999). A circularly permutated fluorescent protein is generated by rearranging the DNA. First, a 5′ region is shifted upstream, toward the start of the gene, creating a new N-terminus in the protein. Secondly, the original C- and N-termini are connected by a flexible linker. The new N- and C-termini have to be in a non-critical position and be flexible (Kostyuk et al., 2019). In the case of cpFPs, the new N- and C-termini are usually located on a region of the β-barrel that, if subjected to conformational rearrangement, causes the whole β-barrel to change its conformation, potentially exposing the chromophore to the external environment with subsequent changes in the photophysics of the chromophore (Kostyuk et al., 2019). cpFPs have been used as sensitive pH sensors (Deng et al., 2021), but the main application is by connecting the new N- and C-termini to a sensing domain for a specific metabolite (Berg et al., 2009; Honda & Kirimura, 2013; Nagai, Sawano, Park, & Miyawaki, 2001) (Fig. 3B). The conformational changes of these domains upon binding or unbinding of the metabolite cause a rearrangement of the β-barrel structure of the cpFPs, which in turn alters the fluorescence spectral properties. Below we discuss in more detail cpFPs specific for the detection of the calcium, potassium, ATP/ADP ratio, NAD(P)H and pH variations.

Another structural modification of FPs is based on the creation of split molecules (Romei & Boxer, 2019), which represent a technological advancement of cpFPs. The structure of split FPs is represented by a

circularly permuted β-barrel in which one of the β-sheets fundamental for the maturation of the chromophore is lacking. Genetically, this can be achieved in the same way as the cpFPs are obtained, with subsequent deletion of the DNA region corresponding to the β-sheet. The β-sheet is then expressed from another plasmid. Once the β-sheet encounters the β-barrel, it complements the structure, allowing for the maturation of the chromophore with subsequent emission of fluorescence. As for normal FPs, the oxidation of the chromophore is the rate limiting step for split-FPs, hence there will be a lag time between the moment in which the β-barrel has been complemented and the emission of fluorescence. Split FPs can be used for different purposes, such as verifying the co-localization of target proteins (Bader et al., 2020) or the co-transcription of target genes (Romei & Boxer, 2019).

4.3 RNA-based sensors

RNA-based sensors have also been developed for detecting small molecules inside cells. These aptamer-based sensors contain a binding domain for the metabolite or signaling molecule, such as cyclic di-AMP (Kellenberger et al., 2015) or cyclic di-GMP (Wang, Wilson, & Hammond, 2016), and an aptamer capable of binding a fluorogenic molecule (Pothoulakis et al., 2014). The aptamer is in an unfolded state prior to the binding of the small molecule. Once the interaction with the analyte occurs, the RNA sensor changes its conformation, allowing the formation of the aptamer and binding of the fluorophore. DFHBI is the main fluorophore used in the so-called Spinach-type structures (Pothoulakis et al., 2014), whereas TO1-biotin is used in Mango-like (Autour et al., 2018). These fluorescent molecules can permeate the cell membrane without affecting the growth of the cells. An advantage of these sensors compared to protein based ones is the rapid detection of metabolites, since the formation of the binding pocket occurs during transcription and does not depend on protein translation and folding.

4.4 FRET-based sensors

FRET sensors can be obtained with any combination of fluorescent molecules, as long as a donor and an acceptor fluorophore are present (Fig. 3A). Co-localization studies can be performed by assessing the presence or absence of FRET between two molecules tagged with a donor and an acceptor (Augustinack et al., 2002). Conformational dynamics studies can be performed by labeling two amino acids on the same protein with a donor

and an acceptor fluorophore and measuring variations in FRET efficiency upon binding of, *e.g.*, a ligand (Götz et al., 2021). Finally, a donor and an acceptor can be connected through a linker containing a sensing domain for specific metabolite, ion or physical factor such as temperature or excluded volume. A change in conformation in this linker will generally result in a change in the positions of the two fluorescent probes relative to one another, bringing them closer together or further apart, depending on the sensor's design (Imamura et al., 2009; Sadoine et al., 2021).

Most genetically encoded FRET sensors use a pair of FPs as donor and acceptors. However, there are three challenges for application of FRET-based sensors: (i) Different fluorescent proteins are affected differently by variations in pH (Campbell, 2001). Hence, one needs to make sure that the pH of cell does not change; (ii) The maturation time of the fluorescent proteins may differ, which affects FRET efficiency (Liu et al., 2018). A possible way to overcome this limitation is by using homo-FRET (Tramier & Coppey-Moisan, 2008). In homo-FRET, the donor and the acceptor are the same molecule, which has the disadvantage that the donor and acceptor cannot be discriminated. However, it is possible to determine variations in fluorescence polarization. When polarized light is used to excite the fluorophore, the emission energy can be transferred via FRET to an identical fluorophore in close proximity. In this energy transfer the emission light gets depolarized, causing a decrease in fluorescence polarization as a function of the distance between two identical fluorophores (Tramier & Coppey-Moisan, 2008). Alternatively, one can use RNA-based FRET sensors, in which two aptamers binding two different dyes change distance upon a conformational change in the sensing domain (Jepsen et al., 2018). These sensors have been used to sense *in vivo* variations in concentrations of small molecules and the detection of specific RNA sequences (Jepsen et al., 2018). (iii) The donor and acceptor can differ in their sensitivity to photobleaching. If the acceptor bleaches more rapidly, then the apparent FRET ratio will be skewed toward lower values. On the contrary, if the donor is more sensitive to bleaching, then the apparent FRET ratio will be higher.

A final note on FRET measurements relates to the environment in which the measurements are performed. It is known that the rate of radiative decay is influenced by the refractive index of the environment (Davidson et al., 2020; Suhling et al., 2002; Tregidgo, Levitt, & Suhling, 2008), and different fluorophores are affected differently by this effect (Borst et al., 2005). Other studies point out a dependency between the time-resolved anisotropy of fluorophores and the viscosity of solutions (Borst et al.,

2005; Suhling, Davis, & Phillips, 2002). If FRET measurements need to be conducted in environments in which the viscosity is expected to change, it is important to consider this effect on the measured FRET efficiency and, if possible, correct the values accordingly.

5. Tracking of molecular and global changes

Fluorescence-based sensors can be used to track a great variety of molecules and physicochemical conditions in the cell (or cell membranes). Such changes can be divided into three categories: (i) detection of molecules, including changes in concentrations of small molecules such as metabolites, ions and signaling molecules; (ii) detection of global changes in the physicochemical properties of the cell such as pH, ionic strength, macromolecular crowding (excluded volume effects), membrane potential, viscosity and volume changes: and (iii) detection of macromolecular interactions and conformational dynamics. The list of available fluorescent sensors is so vast that it is impossible to report them all in a single document. Here, we focus on the tools to track, arguably, the most important molecules and global factors that report the bioenergetics and physicochemistry of the cell and synthetic cell like systems (Table 2).

5.1 Detection of small molecules

Measuring the concentration of specific molecules requires the development of sensors that bind the compound of interest within the expected concentration range and buffer system. In other words, the concentration of the compound must be relatively close to the dissociation constant of the sensor for the molecule. Binding affinities of some sensors, such as ion probes, are often different when measured *in vitro* or *in vivo*. Substrate-binding proteins associated with ATP-binding cassette importers and other types of transporters and ion channels (Scheepers, Nijeholt, & Poolman, 2016) have been a popular source of proteins to which a fluorescence donor and acceptor can be engineered, either by gene fusion with FPs (Isoda et al., 2021; Okumoto, Jones, & Frommer, 2012; Sadoine et al., 2021) or via chemical modification of strategically engineered Cys pairs (de Boer et al., 2019; Gouridis et al., 2015). These proteins are readily engineered to obtain sensors in the appropriate affinity range(s), but other ligand-specific proteins have also been used to design ratiometric or FRET-based sensors (*vide infra*). In addition, we present here a series of chemical probe-based sensors that are taken by

Table 2 List of selected sensors from the main text.

				Spectral maxima (nm)		
Parameter	**Name**	**Fluorophore**	**Read-out**	**Excitation**	**Emission**	**Comments**
Ca^{2+}	Cameleons	BFP, GFP or CFP, YFP	Ratiometric FRET	370 or 440	440, 510 or 480, 535	Multiple versions with varying affinities
Ca^{2+}	Pericam	GFP	Ratiometric	418, 494	511	Intensiometric version available
Ca^{2+}	Fura-2	Stilbene	Ratiometric	340, 380	510	Commercially available
K^+	KIRIN1	mCerulean3 cpVenus	Ratiometric FRET	410	475, 530	Selective for K^+ over Na^+
K^+	KIRIN1-GR	Clover mRuby2	Ratiometric FRET	470	520, 600	Small FRET change
K^+	GINKO1	EGFP	Ratiometric	400, 500	520	Sensitive to high concentrations of Na^+
ATP	Ateam	CFP mVenus	Ratiometric FRET	435	475, 527	Moderately pH sensitive
ATP	GO-Ateam	GFP OFP	Ratiometric FRET	470	510, 560	Red shifted ATeam sensor
ATP	yAT1.03	mTurquoise2 tdTomato	Ratiometric FRET	430	483, 570	pH stable
ATP	Queen	cpEGFP	Ratiometric	400, 494	513	Moderately pH sensitive
ATP/ADP	PercevalHR	cpmVenus	Ratiometric	420, 500	515	pH sensitive
ATP	iATPSnFR	cpSFGFP	Intensiometric	490	512	Ratiometric when fused to mRuby, moderately pH sensitive
ATP	ATPOS	Cy3	Intensiometric	556	566	Hybrid sensor
NADH	Frex	cpYFP	Ratiometric	410, 500	518	pH sensitive

Continued

Table 2 List of selected sensors from the main text.—cont'd

Parameter	Name	Fluorophore	Read-out	Spectral maxima (nm)		Comments
				Excitation	Emission	
$NADH/NAD^+$	Peredox	T-Sapphire mCherry	Ratiometric	400, 575	528, 635	pH stable
$NADH/NAD^+$	SoNar	cpYFP	Ratiometric	420, 485	530	pH insensitive
NADPH	iNAP	cpYFP	Ratiometric	420, 485	530	pH insensitive
Sucrose	FLIPsuc	eCFP eYFP	Ratiometric FRET	435	475, 530	Multiple versions with varying affinities
Cyclic di-AMP	YuaA-Spinac2	Spinach	intensiometric	455	505	RNA-based biosensor
Cyclic di-GMP	Vc2-Spinach	Spinach	intensiometric	455	505	RNA-based biosensor
pH	pHluorin	GFP	Ratiometric	410, 470	535	Intensiometric variant available
pH	pHred	mKeima	Ratiometric	440, 585	610	Compatible with PercevalHR
pH	pyranine	Arylsulfonate	Ratiometric	400, 450	510	Commercially available
pH	BCECF	fluorescein	Ratiometric	439, 490	530	Commercially available
Membrane potential	$DiSC_3$-5	Carbocyanine	Intensiometric	653	676	Commercially available, negative inside potentials
Membrane potential	Oxonol VI	Polymethine	Intensiometric	599	634	Commercially available, positive inside potentials
Viscosity	Various					Various classes available, including ratiometric variants
Vesicle volume/ leakage	Calcein	Fluorescein	Intensiometric	495	520	Self-quenches at high concentrations

Excluded volume	Crowding sensor	Cerulean Citrine	Ratiometric FRET	420	475, 525	Sensors differing in crowding sensitivity are available; different designs available
Excluded volume	Synthetic crowding sensor	Atto488 Atto565	Ratiometric FRET	470, 555	512, 630	Not commercially available
Ionic strength	I-sensor	Cerulean Citrine	Ratiometric FRET	420	475, 525	Different designs available
Temperature	ER thermoyellow		Intensiometric	560	584	Monitor temperature in Enodplasmic Reticulum of eukaryotic cells

Columns are, from left to right: parameter that is sensed by the sensor, name of the sensor, fluorophore(s) used in the sensor, type of sensor (intensiometric, ratiometric or FRET-based), maximum excitation wavelength, maximum emission wavelength, comments on the sensor.

cells via endocytosis or as acetoxymethyl ester derivative. In case of synthetic vesicles or cell-like systems the protein or chemical probe-based sensors are encapsulated in the lumen during the reconstitution procedure.

5.1.1 Calcium sensors

The very first fluorescent genetically encoded sensors were developed to monitor Ca^{2+} ions, which is a key signaling molecule in many cell types (Miyawaki et al., 1997). These FRET-based sensors consist of blue, and green or yellow emitting GFP analogues. Calmodulin fused to the calmodulin-binding peptide of myosin light-chain kinase (M13) are used as Ca^{2+} binding domain. Ca^{2+} binding switches the conformation from an extended to a compact and globular shape, which draws the two fluorophores closer toward each other, increasing the FRET efficiency. Pericam Ca^{2+} sensors have one fluorescent protein (Nagai et al., 2001) and use calmodulin fused to M13 to bind calcium ions. In addition to an intensiometric and an inverted intensiometric sensor (fluorescence intensity decreases upon binding of Ca^{2+}), a ratiometric version is available with an affinity constant for Ca^{2+} binding of 1.7 μM. The Pericam sensors are sensitive toward pH, so care must be taken to keep the pH constant during experiments or to correct for the pH bias.

A popular chemical probe for calcium is Fura-2 (Grynkiewicz, Poenie, & Tsien, 1985). It has high affinity for Ca^{2+} ions ($K_D \sim 0.1\,\mu M$). The excitation spectrum of Fura-2 is ratiometric. Similar to many other chemical dyes, an acetoxymethyl ester form is available, which is membrane-permeable. When used *in vivo*, the ester bond is cleaved intracellularly, which traps the dye inside of the cell.

5.1.2 Potassium and sodium ion sensors

Potassium ions can be measured with protein-based sensors (Shen et al., 2019). KIRIN1, KIRIN1-GR and GINKO1 are sensors based on K^+ binding protein Kbp from *Escherichia coli*. KIRIN1 and KIRIN1-GR are similar in design as a FRET sensor, but differ in fluorophores. KIRIN1 uses CFP and mVenus, while KIRIN1-GR has GFP and mRuby2 as fluorescent proteins. GINKO1 only has a single fluorophore and uses the excitation ratio as readout. As the binding protein is the same for all three sensors, the resulting dissociation constants for K^+ are very similar, *i.e.*, between 0.4 and 2.5 mM, which is well below the physiological levels of potassium in most cells. Here, it would be highly desirable to engineer the sensors toward a lower affinity for K^+ ions (K_D in the 100 mM range)

The measurement of sodium ions is more problematic as no protein-based sensors are available. Some chemical probes have been developed, but they suffer from poor selectivity toward either K^+ or Na^+, poor affinity and an intensiometric readout (Meier, Kovalchuk, & Rose, 2006; Minta & Tsien, 1989; Szmacinski & Lakowicz, 1997). The ions are chelated via crown ethers, ring structures that consist of several ether groups. The size of the crown determines which alkali ion is preferred, but usually multiple ions are accepted. These probes can be useful in a scenario where only one of the two ions is present in the reaction mixture.

5.1.3 ATP sensors

One of the first protein sensors for ATP is ATeam (Imamura et al., 2009), which is a FRET-based sensor. The ε-subunit of the F_0F_1-ATP synthase of *Bacillus subtilis* is flanked by two fluorophores, CFP and mVenus. The latter GFP analogue was circularly permutated to improve the dynamic range of ATP concentrations. Without ATP, the sensor adopts an extended and flexible conformation with low FRET efficiency between the two fluorescent proteins. When ATP is bound, the two fluorophores are drawn closer to each other, causing an increase in acceptor emission. The sensor has a millimolar affinity for ATP and is thus suitable for use with ATP concentrations in the physiological range. By using the ε-subunit of a thermophilic *Bacillus* sp. PS3, the affinity for ATP was increased to the micromolar range. A more pH stable ATP sensor was developed by Botman, van Heerden, and Teusink (2020). The donor fluorophore was replaced by mTurquoise2 and the acceptor with tdTomato, which are both pH stable fluorescent proteins. A newer version of the ATeam sensor, Queen, contains only a single circularly permuted fluorophore (Yaginuma et al., 2014). The Queen sensors have the same affinities for ATP as the ATeam sensors, but are less sensitive to molecular crowding and bleaching.

PercevalHR is an ATP to ADP ratio sensor; it binds both ATP and ADP with similar micromolar affinity (Tantama, Martínez-François, Mongeon, & Yellen, 2013). It consist of a circularly permutated mVenus as the fluorophore, and GlnK as the nucleotide-binding domain. GlnK has a role in ammonia transport in prokaryotes and binds both nucleotides, but only ATP binding stabilizes the conformation of the loop structure near the binding site. This results in increased fluorescence with excitation at 500 nm, whereas ADP binding causes a slight increase in fluorescence with excitation at 420 nm. The ratio between these wavelengths in the excitation spectrum can be used as readout for the ATP to ADP ratio. Knowing the actual

BOX 2 Energy currencies of the cell

All known forms of life use mostly two forms of energy currency: ATP and electrochemical ion gradients. In order describe the energy status of a cell, the concentrations of ATP, ADP and inorganic phosphate and the electrochemical gradients of protons and sodium ions across the membrane need to be measured. The amount of free energy released upon hydrolysis of ATP to ADP plus inorganic phosphate is given by the phosphorylation potential (ΔG_p or $\Delta G_p/F$):

$$\Delta G_p = \Delta G^{0\prime} + 2.3RT log \frac{[ADP][Pi]}{[ATP]} (\mathrm{kJ/mol})$$

$$or\ \frac{\Delta G_p}{F} = \frac{\Delta G^{0\prime}}{F} + \frac{2.3RT}{F}\ log\ \frac{[ADP][Pi]}{[ATP]} (\mathrm{mV})$$

Electrochemical proton or sodium ion gradients are most often used to drive membrane-bound processes, even though other types of ion and solute gradients exist. The F_0F_1-ATP synthase/hydrolase interconverts the free energy of the phosphorylation potential into an electrochemical proton gradient, hereafter referred to as proton motive force (Δp):

$$\Delta \mathrm{p} = \Delta\Psi + \frac{2.3RT}{F}\ log\ \frac{[H^+]_{in}}{[H^+]_{out}} = \Delta\Psi - \mathrm{Z}\Delta\mathrm{pH(mV)}$$

where $2.3RT/F$ equals 58 mV (at T = 298 K) and is abbreviated as Z; F is the Faraday constant, R the gas constant and T is the absolute temperature. $\Delta\Psi$ is the membrane potential, and ΔpH refers to the pH gradient across the membrane. $\Delta G^{0\prime} = -30.5$ kJ/mol, and typically ΔG_p ranges from −50 to −65 kJ/mol (or $\Delta G_p/F$ varies from −520 to −670 mV). A sodium motive force (Δs) can be formed in a similar manner:

$$\Delta \mathrm{s} = \Delta\Psi + \frac{2.3RT}{F}\ log\ \frac{[Na^+]_{in}}{[Na^+]_{out}} = \Delta\Psi - \mathrm{Z}\Delta\mathrm{pNa(mV)}$$

concentrations of ATP and ADP (and inorganic phosphate) is required to calculate the phosphorylation potential (Box 2), which is possible if the sum of ATP plus ADP is known and the ATP/ADP ratio is determined (Pols et al., 2019).

Lastly, ATPOS is a hybrid sensor (Kitajima et al., 2020). Similar to the ATeam and Queen sensor variants, ATPOS uses the ε-subunit of the F_0F_1-ATP synthase of thermophilic *Bacillus* PS3 for ATP binding. The read-out, however, is done by Cy3, a small molecule fluorophore instead of

a fluorescent protein. The resulting sensor has very high affinity for ATP (a K_D of 150 nM) and is insensitive to changes in pH between pH values of 6 and 8.5.

5.1.4 NAD(P)H sensors

The first sensors for NADH and NAD^+/NADH were Frex (Zhao et al., 2011) and Peredox (Hung, Albeck, Tantama, & Yellen, 2011), respectively. Both sensors utilize the bacterial protein Rex, which binds to NADH and regulates metabolism based on the NAD^+/NADH levels (Somerville & Proctor, 2009). Although Rex itself is a homodimeric protein, the sensors contain an in tandem dimeric version. In the Frex sensor, part of one of the monomers is replaced by cpYFP, whereas in Peredox the cpFP is inserted between two complete monomers. Frex reports the NADH concentration with a K_D of 3.7 μM, while Peredox reports the NAD^+ to NADH ratio despite having poor affinity for NAD^+.

Zhao et al. (2015) introduced the NAD^+/NADH ratio sensor SoNar, which is also based on the Rex protein and includes two cpFPs instead of just one. The affinity of SoNar for NADH and NAD^+ differs 20-fold (higher affinity for NADH), which compares to a ±8000 fold difference in Peredox. Therefore, the sensor is sensitive to changes in concentrations of both NADH and NAD^+. Additionally, SoNar is not sensitive to pH changes between pH 7 and 8. The sensor was successfully used in finding compounds that cause oxidative stress in cancer cells.

To be able to measure NADPH levels in cells, the iNAP sensors were developed (Tao et al., 2017). The binding site of SoNar was mutated to selectively bind NADPH instead of NADH by introducing positive charges to accommodate the negative charge of the phosphate group of NADPH and reducing the steric hindrance caused by this group. This resulted in four iNAP sensors with affinities for NADPH varying from 2 to 120 μM.

5.1.5 Metabolite sensors based on substrate-binding proteins

Substrate binding protein (SBP)-based sensors have been developed for many different molecules, including sugars (Otten et al., 2019), amino acids (Ko, Kim, & Lee, 2017) and vitamins (Edwards, 2021). Most are FRET-based sensors, in which a donor and an acceptor are fused to flexible domains of the SBP. These sensors exploit the conformational change of SBPs upon binding of their substrate. The conformational changes can either drive closer or further apart the two fluorescent proteins, with subsequent increases or decreases of FRET.

An example of an SBP-based sensor is the periplasmic leucine-binding protein (LBP) fused to an FP and chemical modified with a fluorescence donor (Ko et al., 2017). The protein was genetically engineered to introduce a fluorescent unnatural amino acid, L-(7-hydroxycoumarin-4-yl) ethylglycine (CouA), which acts as FRET donor, and a YFP as fluorescence acceptor fused to the N-terminus of the protein. The donor and acceptor moieties are brought closer together upon binding of Leu to the LBP, with subsequent increase of FRET.

A recently developed series of sucrose-specific sensors allowed to expand the detection range of sucrose from micro- to millimolar concentrations (Sadoine et al., 2021). In these sensors a sucrose binding protein, ThuE, is genetically engineered by fusing to it an eCFP, which acts as FRET donor, and an eYFP, which acts as FRET acceptor. Binding of sucrose by ThuE drives the two FPs further apart, with subsequent decrease of FRET. The currently available SBP-based sensors are too many to be listed in this work, but we redirect the reader to the review by Specht et al. (Specht et al., 2017) for a more extensive overview.

5.1.6 RNA-based sensors

RNA-based sensors are a new development, and at the writing of this manuscript only a few examples are available. Some recently developed RNA-based fluorescent sensors are capable of sensing variations in concentration of cyclic di-AMP (Kellenberger et al., 2015), cyclic di-GMP (Wang, Wilson, & Hammond, 2016) and cyclic AMP-GMP (Kellenberger, Wilson, Sales-Lee, & Hammond, 2013). The design of RNA-based sensors is based on the presence of an aptamer and a sensing domain. In the unbound state, the aptamer is unfolded. Upon binding of the ligand, the sensor undergoes a conformational change that causes the folding of the aptamer, which can then bind an organic dye and emit fluorescence. The aptamer of currently available sensors are often Spinach- (Pothoulakis et al., 2014) or Broccoli-derived (Filonov, Moon, Svensen, & Jaffrey, 2014). Spinach and Broccoli are two aptamers characterized by a GFP-like emission spectrum upon binding of the organic dye DFHBI.

5.2 Detection of general physicochemical factors

The general physicochemical state of the cell is characterized by the internal pH (the difference in pH between two compartments yields a pH gradient or ΔpH; Box 2), macromolecular crowding (or excluded volume effects), ionic strength, membrane potential (see also Box 2), temperature, volume

and viscosity. These general or global factors impact the growth of any cell and influence the efficiency of biochemical reactions.

5.2.1 pH sensors

pHluorin is one of the first GFP analogues specifically developed to measure pH inside cells (Miesenböck, De Angelis, & Rothman, 1998). The excitation spectrum of wild type GFP is virtually unaffected by changes in pH. By introducing nine mutations, the excitation spectrum displays a change in the ratio of two distinct maxima between pH 5.5 and 7.5. In addition to this ratiometric version, an intensiometric version of pHluorin has been created which loses fluorescence at low pH values.

Another pH sensitive fluorescent protein is pHred (Tantama, Hung, & Yellen, 2011), and this sensor was developed for the simultaneous use with other GFP-based sensors. pHred is based on the RFP mKeima, which has a long Stokes shift. As with pHluorin, the ratio of the intensity of the excitation peaks changes from pH 5.5 to 9. pHred was successfully used simultaneously with PercevalHR (Tantama et al., 2013), which is pH sensitive. The pH data from pHred were used to correct for the influence of pH on the ATP/ADP ratio data reported by PercevalHR (Tantama et al., 2013).

Commercial chemical probes are also available to monitor pH values. These probes allow imaging for longer periods of time compared to the protein-based sensors, because they are less sensitive to photobleaching. Both Pyranine (Kano & Fendler, 1978) and BCECF (James-Kracke, 1992) are ratiometric and have pK_a values of 7.2 and 7.0, respectively. The BCECF-AM derivative can be used to introduce and trap BCECF in living cells.

5.2.2 Membrane potential sensors

The membrane potential is one of the components of the proton and sodium motive force (Box 2) and an important energy currency of all cells. It is used as driving force (often in combination with a pH or sodium gradient) for numerous membrane-bound processes such as the synthesis of ATP, solute transport, reverse electron transport, protein translocation and others. The membrane potential can be measured with chemical probes such as $DiSC_3(5)$ (Sims, Waggoner, Wang, & Hoffman, 1974). $DiSC_3(5)$ or 3,3′-Dipropylthiadicarbocyanine Iodide belongs to the group of so-called Nernstian probes that have a delocalized positive charge. The monomeric form of the probe is fluorescent, and the molecule distributes between the extracellular medium and the lipid membrane. In vesicle suspensions

without applied membrane potential the dye distributes between the extracellular medium and the lipid membrane. Upon hyperpolarization of the membrane the dye will accumulate on the side of membrane where the potential is negative and dimers and higher order aggregates will form, resulting in a decrease in fluorescence. When the vesicles are depolarized the dye redistributes over both membrane leaflets and is partially released back into the extracellular medium.

Oxonol VI is a similar probe as $DiSC_3(5)$, but has a negative charge instead (Apell & Bersch, 1987). Therefore this dye is suited for measuring inside positive membrane potentials. Upon polarization (inside positive), the fluorescence increases, in contrast to the decrease in fluorescence of $DiSC_3(5)$ upon the formation of inside negative potentials.

5.2.3 Viscosity

Viscosity can be measured using fluorescent molecular rotors (Kuimova, 2012; Lee et al., 2018; Liu et al., 2020). When excited, these sensors can either relax to a lower energy state by emitting a photon, or adopting a twisted intramolecular charge transfer (TICT) state. Part of the molecule rotates to adopt this TICT state and the rotation process is affected by viscosity. At high viscosity the TICT state is less favorable, thus fluorescence is increased. Depending on the probe used, fluorescent lifetime, the emission intensity or the ratio of maxima in the emission spectrum can be used as readout.

5.2.4 Volume sensing

When subjected to an osmotic shock or upon the transport of large amounts of solutes over the membrane, the size of a cell or vesicle will change. While the size of cells can be measured by microscopy, this is not possible for very small cells or, *e.g.*, large-unilamellar vesicles with diameters in the range from 100 to 200 nm, which is below the diffraction limit. Therefore the size of these vesicles can only be measured by indirect methods. A way to measure vesicle size is by taking advantage of the self-quenching characteristics of fluorophores. When dyes like Calcein are encapsulated at high (approximately 10 mM) self-quenching concentrations, the fluorescence readout signal becomes dependent of the volume of the compartment. When the internal volume decreases, the calcein fluorescence decreases; similarly, the signal increases when the vesicles swell (Gabba et al., 2020; van der Heide, Stuart, & Poolman, 2001).

5.2.5 Excluded volume sensors

Excluded volume or macromolecular crowding can affect the conformation of proteins and reactions' efficiency (van den Berg, Boersma, & Poolman, 2017). The excluded volume is the volume taken by all the macromolecules of the cell, which is therefore not available for a given molecule added to the system. Compaction of a macromolecule by, *e.g.*, the coming closer of two or more protein domains is favoured due to an entropic gain. This principle was used to develop FRET sensors capable of probing the excluded volume of the cell (Boersma, Zuhorn, & Poolman, 2015; Liu et al., 2017, 2018). The genetically encoded sensors consist of mCitrine (YFP, yellow fluorescent protein) and mCerulean (CFP, cyan fluorescent protein), which are connected via a flexible linker, including two α-helices. At high excluded volume levels the sensor adopt a more condensed conformation, bringing the two fluorophores closer to each other, which is observed as an increase in apparent FRET efficiency. In a follow up study, a set of nine systematically varied sensors have been developed and the crowding-induced compression of the proteins has been investigated (Liu et al., 2017).

Using the same principle, a sensor has been created from a polymer linker coupled to synthetic fluorophores (Gnutt, Gao, Brylski, Heyden, & Ebbinghaus, 2015). Here, the linker consists of a 10 kDa PEG molecule, labelled with Atto488 and Atto565 at either end of the polymer. Both the genetically encoded and polymer-linked probe sensors are especially sensitive to crowding by macromolecules or synthetic polymers.

5.2.6 Ionic strength sensors

Ionic strength can be measured via a FRET-based sensor that acts similarly to the macromolecular crowding sensor (Liu, Poolman, & Boersma, 2017). This sensor also consists of two fluorescent proteins joined by a flexible linker. Here, the linker consists of two α-helices with opposite charges. At low ionic strength levels, the opposite charges of the helices attract each other, increasing the FRET efficiency. At higher ionic strength levels, the charges of the linker are shielded by ions, which allows the FPs to stay further apart, which lowers the apparent FRET ratio.

5.2.7 Temperature sensors

Temperature in solutions or in living cells can be measured using chemical probes. Different probes have recently been developed (Arai, Lee, Zhai, Suzuki, & Chang, 2014; Maksimov et al., 2019; Okabe et al., 2012), and of particular interest for physiological studies is the use of

polymer-encapsulated quantum dots (Fan et al., 2015), which show a high resistance to pH and ionic strength changes in the physiological range. They can enter mammalian cells by endocytosis but they have not been applied in lower eukaryotes or prokaryotes.

5.3 Detection of macromolecular interactions and conformational dynamics

Fluorescent tools are typically used to track changes in molecular interactions, localization, conformation and concentration. Localization of macromolecules can be achieved by adding a fluorescent tag to the molecule of interest (Chalfie et al., 1994; van Berkel et al., 2011). This strategy has also been employed to study proteins and RNA turnover (Trauth et al., 2020). Interactions between macromolecules can be observed by tagging different putative interacting partners with different fluorescent reporters and subsequently measuring the FRET efficiency, which will increase as a function of the proximity of the two fluorescent molecules (Kaufmann et al., 2020). In a similar way, changes in conformation of macromolecules can be studied via FRET measurements by tagging with different fluorescent reporters different parts of the analyzed macromolecules (Götz et al., 2021). We refer to a set of papers (Ploetz et al., n.d.; Asher et al., 2021; de Boer et al., 2019; Lerner et al., 2021) for determining interactions between macromolecules and conformational dynamics within proteins.

6. Microscopy techniques

In this section we present some of the most common techniques to measure the fluorescence of the sensors reported heretofore, highlighting the differences and the advantages and disadvantages of the various methods. Reporting all possible fluorescence detection methods would be beyond the scope of this review, and for a more thorough characterization of the available techniques we redirect the reader to different works (Combs, 2010; Datta, Heaster, Sharick, Gillette, & Skala, 2020; Huang, Bates, & Zhuang, 2009; Lichtman & Conchello, 2005; Renz, 2013).

For most *in vitro* (in solution or in vesicles) measurements, a spectrophotometer is typically used. A spectrophotometer allows exciting a sample at a specific wavelength or range of wavelengths and acquires the emission at the desired wavelength or range of wavelengths. It can be used to analyze both the emission and the excitation spectra, and it is fundamental to study how the spectra of fluorescent probes are affected by changes in the environment.

Time Correlated Single Photon Counting (TCSPC) allows obtaining information about the lifetime of the fluorescent species in a solution (Phillips, Drake, O'Connor, & Christensen, 1985), to perform different *in vitro* studies, such as accurately determining the FRET efficiency of a FRET pair, or measuring the viscosity of a solution with molecular rotors (Liu et al., 2020).

Fluorescence microscopy, on the other hand, is the most utilized technique for *in vivo* measurements, as it allows obtaining spatial information on the localization of the analyzed probes.

6.1 Confocal microscopy

Confocal microscopy is an imaging technique that allows increased contrast and resolution of a micrograph compared to classical fluorescence microscopy (Jonkman, Brown, Wright, Anderson, & North, 2020). Confocal microscopes use point illumination in combination with a pinhole to filter out the out-of-focus signal. This allows obtaining images at higher resolution (yet still diffraction limited), at the cost of reduced emission intensity. Such limitation can be overcome by increasing the pinhole size (hence lowering the resolution), increase the exposure time (hence encountering the possibility of blurring effects due to particles diffusion) or using probes with high brightness and quantum yield.

Since only a single point is illuminated in the field of view, confocal microscopy requires 2D scanning of the confocal plane to obtain an image. The confocal plane can then be moved along the z-axis, allowing to obtain multiple 2D images across the same sample, which can then be stacked together to obtain a 3D reconstruction of the sample (Jonkman et al., 2020). Other than for imaging purposes, confocal microscopes can be used to perform different types of measurements as summarized in the next subsections.

6.1.1 Fluorescence recovery after photobleaching

Fluorescence recovery after photobleaching (FRAP) (Carnell, Macmillan, & Whan, 2015) is a technique used to study diffusion and interactions of macromolecules, hence it can be used to determine whether a sensor is freely diffusing or if it is confined within specific regions of the cell. Briefly, a high intensity laser pulse at the excitation wavelength of the imaged probe is used to bleach a region of the imaged sample. Once bleached (see Box 1), the probes localized in that region undergo a structural change and lose the ability to emit photons. The bleached region appears dark upon bleaching of the probes, and gradually the fluorescence increases due to

the diffusion of undamaged probes into the bleached are. The kinetics of the recovery of fluorescence can be used to calculate the ensemble diffusion coefficient and the fraction of freely diffusing macromolecules. Due to their lower photostability and tendency to rapidly photobleach, FPs can be more suitable for FRAP experiments in living cells than photostable dyes. FRAP can be used to track diffusion of proteins in the cytoplasm (Mika, Krasnikov, van den Bogaart, de Haan, & Poolman, 2011; Schavemaker, Śmigiel, & Poolman, 2017) and in the cell membrane (Goehring, Chowdhury, Hyman, & Grill, 2010) of both eukaryotic and prokaryotic cells, and in small compartments of eukaryotes such as mitochondria (Sukhorukov et al., 2010). At the same time, it has also been proven useful to track diffusion in various membrane environments such as lipid bilayers (Pincet et al., 2016), and giant-unilamellar vesicles (Göpfrich et al., 2019).

6.1.2 Fluorescence lifetime imaging microscopy

Fluorescence lifetime imaging microscopy (FLIM) (Datta et al., 2020) allows measuring the lifetime of the excited fluorescent probes, which is important for establishing that the probes in FRET-based sensors are freely rotating (see Section 4.4). FLIM employs pulsed illumination, using ultrashort pulses of light. TCSPC equipment is required for obtaining pulses at a sub-picosecond time resolution. The time between the laser pulse and the emission of the photon by the fluorescent probe can then be calculated. Thereby information is obtained on the permanence of the fluorophore in the excited state. Billions of data points are accumulated over a short period of time and then used to generate a histogram that follows a Poisson distribution (Datta et al., 2020). The data points are then fitted with an exponential model, which allows determining the fluorescence lifetime of the sample and the eventual presence of multiple lifetimes (Poudel, Mela, & Kaminski, 2020). Multiple lifetimes can be observed when the probes are present in different conformational states (Borst et al., 2005). FLIM can be used to study protein dynamics (Sun, Hays, Periasamy, Davidson, & Day, 2012) and the environmental conditions of solutions and cells, using lifetime-based probes. In these probes it is not the shape of the excitation or emission spectra that change in response to variations in the measured parameter, rather it is the lifetime of the fluorescent molecule. FLIM is also commonly used to measure FRET efficiencies *in vivo* via FLIM-FRET (see Section 6.3). Lifetime of fluorescent molecules can be affected by changes in the environment (Kashirina et al., 2020) or by changes in the

structure of the fluorescent molecule itself (Hirata, Hirakawa, Shimada, Watanabe, & Ohtsuki, 2021), allowing for the development of probes that can sense environmental changes or molecular changes.

6.2 Super resolution microscopy

Super resolution microscopy encompass a set of techniques that allow obtaining wide-field images of the analyzed probes at a resolution level beyond the diffraction limit via detection of single molecules (Khater, Nabi, & Hamarneh, 2020). Detection of single molecules can be achieved by using Total Internal Reflection Fluorescence (TIRF) microscopes (Fish, 2009), which use a source of light to illuminate the sample at a sufficiently oblique angle such that the light wave is totally reflected without refraction into the sample, allowing to image a very thin region of the cell, usually less than 200 nm. TIRF is an extremely powerful technique to image fluorescently labeled molecules that are in the vicinity of the glass slide onto which the cell or vesicle sample is loaded (Fish, 2009). To measure fluorescence deeper inside the vesicles or cells, it is necessary for the light to pass through the sample and excite the fluorescent probes in a confined area. A technique called Highly Inclined and Laminated Optical sheet (HILO) microscopy (Tokunaga, Imamoto, & Sakata-Sogawa, 2008) can be used to achieve single-molecule images in these areas. Here the light beam encounters the sample at an angle slightly below the critical angle for total internal reflection, allowing for some light to be refracted into the sample, increasing the image intensity and decreasing background fluorescence (Tokunaga et al., 2008).

There are several super-resolution optical microscopy techniques and here we describe the ones that we are frequently using in conjunction with the probing of the physicochemical state of the cells with the heretofore-reported sensors.

6.2.1 Photo-activated localization microscopy and stochastic optical reconstruction microscopy

Photo-activated localization microscopy (PALM) (Gould, Verkhusha, & Hess, 2009) and Stochastic Optical Reconstruction Microscopy (STORM) (Rust, Bates, & Zhuang, 2006) are both based on the use of photoblinking of fluorescent molecules, such as photoactivatable or photoswitchable FPs or fluorescent dyes. Photoblinking allows obtaining spatially separated spots of fluorescence, thereby overcoming the diffraction limit (Khater et al., 2020). Briefly, a low intensity laser pulse of the proper wavelength

is used to stochastically photoactivate a few fluorescent molecules, converting their fluorophore from its inactive-OFF to its active-ON state. A second laser pulse is then used to excite the active fluorescent molecule and its emission is measured as a single distinguishable spot. Laser pulses are spaced at milliseconds intervals and repeated for thousands of frames, allowing detecting multiple single molecules (Khater et al., 2020). After measuring its emission, the fluorescent molecule can then either be brought back to its OFF-inactive state by a third laser pulse at the proper wavelength (Wazawa et al., 2021) or photobleached, to avoid recording the same molecule more than once. In the case of photobleaching, it is necessary to ensure a high concentration of fluorescent molecule prior of the experiment, such as with a high expression system in the case of FPs, as the number of activated molecules will decrease over time. The single spots are then analyzed and a spatial map at resolution well beyond the diffraction limit of light is obtained. Stacking together all the acquired frames allows obtaining a super-resolution image. Recent advancements allowed to reconstruct super resolution 3D images, for example by assigning a different z coordinate to a spot as a function of its intensity (Huang, Wang, Bates, & Zhuang, 2008).

6.2.2 Single molecule displacement mapping

Single molecule displacement mapping (SMDM) (Xiang, Chen, Yan, Li, & Xu, 2020) is a recently developed technique that allows obtaining maps of diffusion coefficients at a nanometer scale resolution, providing an insight on how static structures or interactions affect the motion of particles *in vitro* and in living cells (Xiang et al., 2020). Briefly, photoactivable FPs are stochastically switched to their active-ON state by a short laser pulse of low intensity and the proper wavelength. Subsequently, two short pulses that excite the active FPs at a short time distance from each other allow monitoring the position of the same FP at two distinct moments. Knowing the time step and the displacement allows to reconstruct the diffusion coefficient by fitting a probability distribution function for a two dimensional random walk (Eq. 9):

$$p(x,t) = \frac{2r}{4Dt} e^{-\frac{r^2}{4Dt}} + kr \tag{9}$$

where t is the time step, r is the displacement, k is a factor used to correct for the background fluorescence, and D is the lateral diffusion coefficient. This technique allows observing heterogeneities in diffusion at single molecule resolution, which may reveal static structures or confined regions in the cell (Xiang et al., 2020).

6.3 FRET imaging

Confocal FRET imaging allows measuring the fluorescence intensity of donor and acceptor separately, which are then used to calculate the apparent FRET efficiency as in Eq. (1). This technique is used to perform colocalization (Augustinack et al., 2002) and interaction (Margineanu et al., 2016) studies. The FRET signal is sensitive to the concentration of sensor molecule analyzed. Moreover, fluorescent molecules with partially overlapping emission spectra can lead to a lower apparent FRET efficiency. Therefore, if FRET efficiency is used for quantitative measurements, such as with FRET-based biosensors, we believe that FLIM-FRET is a more powerful tool as it is not dependent on the concentration of the fluorescent species and only requires measurement of the donor lifetime (Periasamy et al., 2015). With this technique it is possible to calculate the exact FRET efficiency of a FRET pair, as per Eq. (6). A drawback of this method, however, is the necessity of having to measure the lifetime of the donor alone, isolated from the FRET pair. Since the lifetime and the anisotropy decay of fluorescent molecules, in particular of fluorescent proteins, are dependent on the environment (Borst et al., 2005; Suhling, Davis, & Phillips, 2002), it is not possible to use *in vitro*-obtained values of the donor's lifetime, but it is necessary to measure the donor's lifetime in the same system in which the FRET pair is analyzed.

7. A map to navigate the fluorescent sea

The amount of fluorescent tools and available techniques to detect them is extremely vast. Depending on the requirements and the condition of a specific study, one should accurately choose the proper probe and the proper method. However, finding the proper tool with the right characteristic and pairing it with the proper technique can be overwhelming, as many factors need to be taken into account: is the study going to be performed *in vitro* or *in vivo*? Is the environmental pH going to change? Are other environmental parameters such as the viscosity expected to change? Is the experiment going to be based on photobleaching? Will the study assess quantitative FRET changes as a function of variations in the concentration of metabolites? Recently, an algorithm for the selection of fluorescent reporters depending on the instrument settings has been published (Vaidyanathan et al., 2021), helping in the choice of the fluorescent molecules as a function of their spectral properties. Below (Fig. 4) we consider the

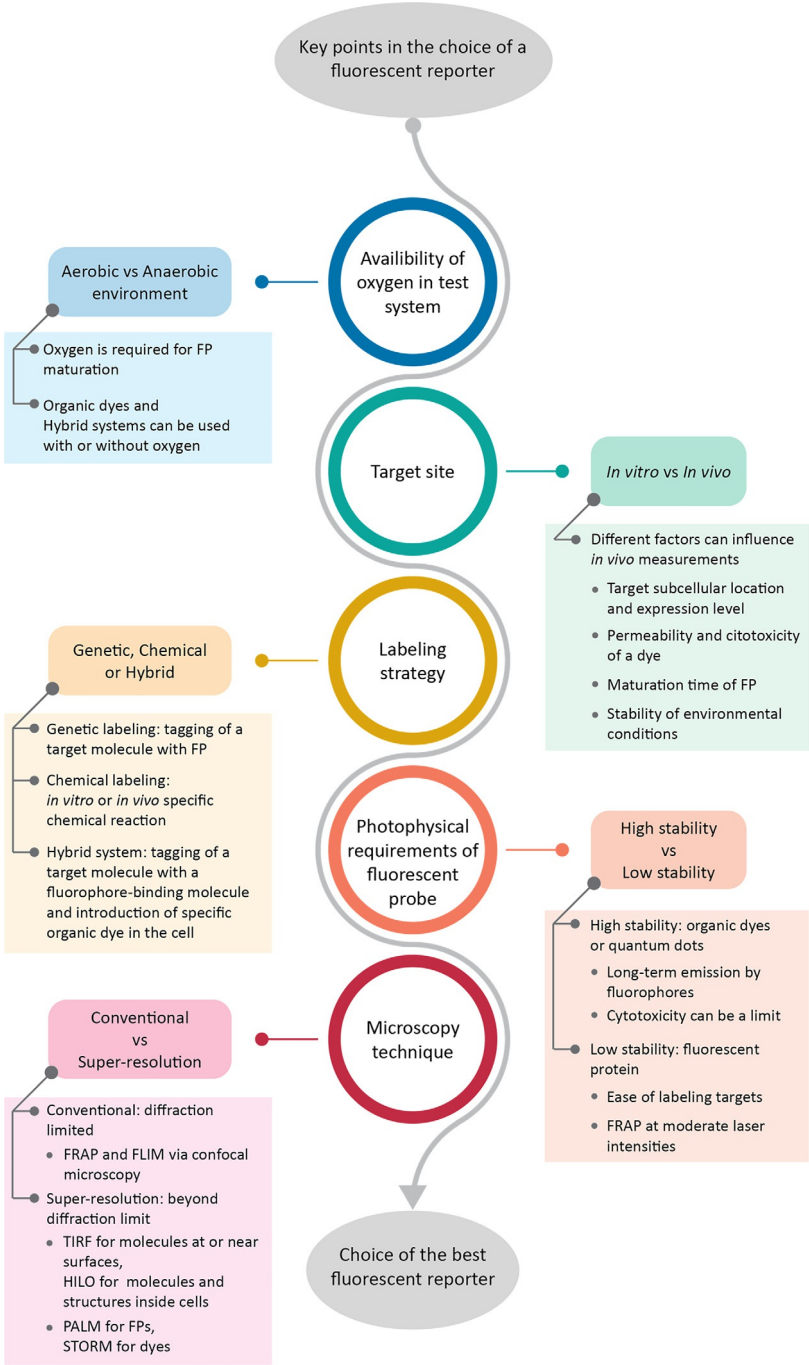

Fig. 4 Important points to consider when choosing a fluorescent reporter.

problem from a broader perspective, and we provide a flowchart of the important steps to consider for fluorescence-based sensing of living cells or artificial systems.

8. Conclusions

The field of biological fluorescence has evolved rapidly. New tools are constantly being developed, and new techniques allow obtaining more accurate data. In this review we have tried to summarize the state of the art on fluorescent probes used for studying the physicochemical state of the cell, be it a living cell, vesicle or cell-like system. We have tried to give a complete, yet very brief overview of the most useful methods for biological imaging. Finally, we provided a series of guidelines to help in the choice of the proper fluorescent tool and imaging technique depending on the purpose of the study.

Although the field of fluorescence probes and fluorescence microscopy has made huge steps forward in the last several years, we are approaching the limits of the possibilities provided by these instruments. While more and more molecules will be detected by the development of new molecule-specific sensors, answering questions on the general chemical physical status of a cell at high spatiotemporal resolution has proven to be much more complicated. Recently developed techniques such as SMDM allow obtaining detailed spatial information in living cells, while single molecule FRET allows observing heterogeneities in the FRET efficiency within the same system. These methods, however, pose technical hurdles that need to be overcome before application on systems scale is possible. Yet, the future lies in the high-throughput biochemical analysis of the cell at high spatiotemporal resolution, for which the further development of fluorescence-based sensors and methods will remain crucial.

Acknowledgments

The research was funded by an ERC Advanced grant (ABCVolume; #670578) and the EU Marie-Curie ITN project SynCrop (project number 764591).

References

Agouridas, V., et al. (2019). Native chemical ligation and extended methods: Mechanisms, catalysis, scope, and limitations. *Chemical Reviews*, *119*, 7328–7443.

Alexa Fluor. (2021). *Alexa fluor dyes spanning the visible and infrared spectrum—Section 1.3—NL*. www.thermofisher.com/uk/en/home/references/molecular-probes-the-handbook/fluorophores-and-their-amine-reactive-derivatives/alexa-fluor-dyes-spanning-the-visible-and-infrared-spectrum.html.

Allen, T. M., & Cleland, L. G. (1980). Serum-induced leakage of liposome contents. *Biochimica et Biophysica Acta (BBA) - Biomembranes*, *597*, 418–426.
Ando, R., Hama, H., Yamamoto-Hino, M., Mizuno, H., & Miyawaki, A. (2002). An optical marker based on the UV-induced green-to-red photoconversion of a fluorescent protein. *Proceedings of the National Academy of Sciences*, *99*, 12651–12656.
Apell, H.-J., & Bersch, B. (1987). Oxonol VI as an optical indicator for membrane potentials in lipid vesicles. *Biochimica et Biophysica Acta (BBA) - Biomembranes*, *903*, 480–494.
Arai, S., Lee, S.-C., Zhai, D., Suzuki, M., & Chang, Y. T. (2014). A molecular fluorescent probe for targeted visualization of temperature at the endoplasmic reticulum. *Scientific Reports*, *4*, 6701.
Asher, W. B., et al. (2021). Single-molecule FRET imaging of GPCR dimers in living cells. *Nature Methods*, *18*, 397–405.
Augustinack, J. C., Sanders, J. L., Tsai, L.-H., & Hyman, B. T. (2002). Colocalization and fluorescence resonance energy transfer between cdk5 and AT8 suggests a close association in pre-neurofibrillary tangles and neurofibrillary tangles. *Journal of Neuropathology and Experimental Neurology*, *61*, 557–564.
Autour, A., et al. (2018). Fluorogenic RNA mango aptamers for imaging small non-coding RNAs in mammalian cells. *Nature Communications*, *9*, 656.
Bader, G., et al. (2020). Assigning mitochondrial localization of dual localized proteins using a yeast Bi-Genomic Mitochondrial-Split-GFP. *eLife*, *9*, e56649.
Bajar, B. T., Wang, E. S., Zhang, S., Lin, M. Z., & Chu, J. (2016). A guide to fluorescent protein FRET pairs. *Sensors*, *16*, 1488.
Balleza, E., Kim, J. M., & Cluzel, P. (2018). Systematic characterization of maturation time of fluorescent proteins in living cells. *Nature Methods*, *15*, 47–51.
Balzarotti, F., et al. (2017). Nanometer resolution imaging and tracking of fluorescent molecules with minimal photon fluxes. *Science*, *355*(6325), 606–612.
Barondeau, D. P., Kassmann, C. J., Tainer, J. A., & Getzoff, E. D. (2005). Understanding GFP chromophore biosynthesis: Controlling backbone cyclization and modifying post-translational chemistry. *Biochemistry*, *44*, 1960–1970.
Barondeau, D. P., Putnam, C. D., Kassmann, C. J., Tainer, J. A., & Getzoff, E. D. (2003). Mechanism and energetics of green fluorescent protein chromophore synthesis revealed by trapped intermediate structures. *Proceedings of the National Academy of Sciences*, *100*, 12111–12116.
Barreto-Chang, O. L., & Dolmetsch, R. E. (2009). Calcium imaging of cortical neurons using fura-2 AM. *Journal of Visualized Experiments*, *23*, e1067. https://doi.org/10.3791/1067.
Berg, J., Hung, Y. P., & Yellen, G. (2009). A genetically encoded fluorescent reporter of ATP/ADP ratio. *Nature Methods*, *6*, 161–166.
Bittermann, M. R., Grzelka, M., Woutersen, S., Brouwer, A. M., & Bonn, D. (2021). Disentangling nano- and macroscopic viscosities of aqueous polymer solutions using a fluorescent molecular rotor. *Journal of Physical Chemistry Letters*, *12*, 3182–3186.
BODIPY. (2021). *Dye series—Section 1.4—NL*. www.thermofisher.com/uk/en/home/references/molecular-probes-the-handbook/fluorophores-and-their-amine-reactive-derivatives/bodipy-dye-series.html.
Boens, N., et al. (2006). Photophysics of the fluorescent pH indicator BCECF. *The Journal of Physical Chemistry. A*, *110*, 9334–9343.
Boersma, A. J., Zuhorn, I. S., & Poolman, B. (2015). A sensor for quantification of macromolecular crowding in living cells. *Nature Methods*, *12*, 227–229.
Borst, J. W., Hink, M. A., van Hoek, A., & Visser, A. J. W. G. (2005). Effects of refractive index and viscosity on fluorescence and anisotropy decays of enhanced cyan and yellow fluorescent proteins. *Journal of Fluorescence*, *15*, 153–160.

Botman, D., van Heerden, J. H., & Teusink, B. (2020). An improved ATP FRET sensor for yeast shows heterogeneity during nutrient transitions. *ACS Sensors*, *5*, 814–822.
Brakemann, T., et al. (2011). A reversibly photoswitchable GFP-like protein with fluorescence excitation decoupled from switching. *Nature Biotechnology*, *29*, 942–947.
Braut-Boucher, F., et al. (1995). A non-isotopic, highly sensitive, fluorimetric, cell-cell adhesion microplate assay using calcein AM-labeled lymphocytes. *Journal of Immunological Methods*, *178*, 41–51.
Calamera, G., et al. (2019). FRET-based cyclic GMP biosensors measure low cGMP concentrations in cardiomyocytes and neurons. *Communications Biology*, *2*, 1–12.
Campbell, T. (2001). *The Effect of pH on Green Fluorescent Protein: A Brief Review*. undefined.
Campbell, B. C., et al. (2020). mGreenLantern: A bright monomeric fluorescent protein with rapid expression and cell filling properties for neuronal imaging. *Proceedings of the National Academy of Sciences*, *117*, 30710–30721.
Carnell, M., Macmillan, A. & Whan, R. Fluorescence recovery after photobleaching (frap): Acquisition, analysis, and applications. in Methods in Membrane Lipids (ed. Owen, D. M.) 255–271 (Springer, 2015). doi:10.1007/978-1-4939-1752-5_18.
Chalfie, M., Tu, Y., Euskirchen, G., Ward, W. W., & Prasher, D. C. (1994). Green fluorescent protein as a marker for gene expression. *Science*, *263*, 802–805.
Chamberlain, C., & Hahn, K. M. (2000). Watching proteins in the wild: Fluorescence methods to study protein dynamics in living cells. *Traffic*, *1*, 755–762.
Choi, H., Yang, Z., & Weisshaar, J. C. (2015). Single-cell, real-time detection of oxidative stress induced in Escherichia coli by the antimicrobial peptide CM15. *Proceedings of the National Academy of Sciences*, *112*, E303–E310.
Chudakov, D. M., Matz, M. V., Lukyanov, S., & Lukyanov, K. A. (2010). Fluorescent proteins and their applications in imaging living cells and tissues. *Physiological Reviews*, *90*, 1103–1163.
Cole, N. B. (2013). Site-specific protein labeling with SNAP-tags. *Current Protocols in Protein Science*, *73*, 30.1.1–30.1.16.
Collot, M., Boutant, E., Fam, K. T., Danglot, L., & Klymchenko, A. S. (2020). Molecular tuning of styryl dyes leads to versatile and efficient plasma membrane probes for cell and tissue imaging. *Bioconjugate Chemistry*, *31*, 875–883.
Combs, C. A. (2010). Fluorescence microscopy: A concise guide to current imaging methods. *Current Protocols in Neuroscience*, *50*, 2.1.1–2.1.14.
Costantini, L. M., et al. (2015). A palette of fluorescent proteins optimized for diverse cellular environments. *Nature Communications*, *6*, 7670.
Cummings, R. T., et al. (2002). A peptide-based fluorescence resonance energy transfer assay for Bacillus anthracis lethal factor protease. *Proceedings of the National Academy of Sciences*, *99*, 6603–6606.
Darfeuille, F., Hansen, J. B., Orum, H., Primo, C. D., & Toulmé, J. (2004). LNA/DNA chimeric oligomers mimic RNA aptamers targeted to the TAR RNA element of HIV-1. *Nucleic Acids Research*, *32*, 3101–3107.
Datta, R., Heaster, T. M., Sharick, J. T., Gillette, A. A., & Skala, M. C. (2020). Fluorescence lifetime imaging microscopy: Fundamentals and advances in instrumentation, analysis, and applications. *Journal of Biomedical Optics*, *25*, 071203.
Davidson, M. N., et al. (2020). Measurement of the fluorescence lifetime of GFP in high refractive index levitated droplets using FLIM. *Physical Chemistry Chemical Physics*, *22*, 14704–14711.
Day, R. N., & Schaufele, F. (2008). Fluorescent protein tools for studying protein dynamics in living cells: A review. *Journal of Biomedical Optics*, *13*, 031202.
de Boer, M., et al. (2019). Conformational and dynamic plasticity in substrate-binding proteins underlies selective transport in ABC importers. *eLife*, *8*, e44652.

Deng, W., Shi, X., Tjian, R., Lionnet, T., & Singer, R. H. (2015). CASFISH: CRISPR/Cas9-mediated in situ labeling of genomic loci in fixed cells. *Proceedings of the National Academy of Sciences*, *112*, 11870–11875.

Deng, H., et al. (2021). Genetic engineering of circularly permuted yellow fluorescent protein reveals intracellular acidification in response to nitric oxide stimuli. *Redox Biology*, *41*, 101943.

Dirks, R. W., & Tanke, H. J. (2006). Advances in fluorescent tracking of nucleic acids in living cell. *BioTechniques*, *40*, 489–496.

Dorta, D. A., Deniaud, D., Mével, M., & Gouin, S. G. (2020). Tyrosine conjugation methods for protein labelling. *Chemistry - A European Journal*, *26*, 14257–14269.

Edwards, K. A. (2021). Periplasmic-binding protein-based biosensors and bioanalytical assay platforms: Advances, considerations, and strategies for optimal utility. *Talanta Open*, *3*, 100038.

Fan, Y., et al. (2015). Extremely high brightness from polymer-encapsulated quantum dots for two-photon cellular and deep-tissue imaging. *Scientific Reports*, *5*, 9908.

Filonov, G. S., Moon, J. D., Svensen, N., & Jaffrey, S. R. (2014). Broccoli: Rapid selection of an RNA mimic of green fluorescent protein by fluorescence-based selection and directed evolution. *Journal of the American Chemical Society*, *136*, 16299–16308.

Fish, K. N. (2009). Total internal reflection fluorescence (TIRF) microscopy. *Current Protocols in Cytometry/Editorial Board, J Paul Robinson, Managing Editor. [et al]*, *12*. Unit 12.18.

Förster, T. (1948). Zwischenmolekulare Energiewanderung und Fluoreszenz. *Annals of Physics*, *437*, 55–75.

Fu, Y., & Finney, N. S. (2018). Small-molecule fluorescent probes and their design. *RSC Advances*, *8*, 29051–29061.

Gabba, M., et al. (2020). Weak acid permeation in synthetic lipid vesicles and across the yeast plasma membrane. *Biophysical Journal*, *118*, 422–434.

Gauer, J. W., et al. (2016). Chapter ten—Single-molecule FRET to measure conformational dynamics of DNA mismatch repair proteins. In M. Spies, & Y. R. Chemla (Eds.), *581. Methods in Enzymology* (pp. 285–315). Academic Press.

Gautier, A., et al. (2008). An engineered protein tag for multiprotein labeling in living cells. *Chemistry & Biology*, *15*, 128–136.

Gnutt, D., Gao, M., Brylski, O., Heyden, M., & Ebbinghaus, S. (2015). Excluded-volume effects in living cells. *Angewandte Chemie, International Edition*, *54*, 2548–2551.

Goehring, N. W., Chowdhury, D., Hyman, A. A., & Grill, S. W. (2010). FRAP analysis of membrane-associated proteins: Lateral diffusion and membrane-cytoplasmic exchange. *Biophysical Journal*, *99*, 2443–2452.

Göpfrich, K., et al. (2019). One-pot assembly of complex giant unilamellar vesicle-based synthetic cells. *ACS Synthetic Biology*, *8*, 937–947.

Götz, C., et al. (2021). Conformational dynamics of the dengue virus protease revealed by fluorescence correlation and single-molecule FRET studies. *The Journal of Physical Chemistry B*, *125*, 6837–6846.

Gould, T. J., Verkhusha, V. V., & Hess, S. T. (2009). Imaging biological structures with fluorescence photoactivation localization microscopy. *Nature Protocols*, *4*, 291–308.

Gouridis, G., et al. (2015). Conformational dynamics in substrate-binding domains influences transport in the ABC importer GlnPQ. *Nature Structural & Molecular Biology*, *22*, 57–64.

Gray, W. D., Mitchell, A. J., & Searles, C. D. (2015). An accurate, precise method for general labeling of extracellular vesicles. *MethodsX*, *2*, 360–367.

Grynkiewicz, G., Poenie, M., & Tsien, R. Y. (1985). A new generation of Ca2 + indicators with greatly improved fluorescence properties. *The Journal of Biological Chemistry*, *260*, 3440–3450.

Guo, M., Xu, Y., & Gruebele, M. (2012). Temperature dependence of protein folding kinetics in living cells. *Proceedings of the National Academy of Sciences*, *109*, 17863–17867.
Haupts, U., Maiti, S., Schwille, P., & Webb, W. W. (1998). Dynamics of fluorescence fluctuations in green fluorescent protein observed by fluorescence correlation spectroscopy. *Proceedings of the National Academy of Sciences of the United States of America*, *95*, 13573–13578.
Hebisch, E., Knebel, J., Landsberg, J., Frey, E., & Leisner, M. (2013). High variation of fluorescence protein maturation times in closely related escherichia coli strains. *PLoS One*, *8*, e75991.
Heim, R., Prasher, D. C., & Tsien, R. Y. (1994). Wavelength mutations and posttranslational autoxidation of green fluorescent protein. *Proceedings of the National Academy of Sciences*, *91*, 12501–12504.
Henderson, J. N., et al. (2009). Structure and mechanism of the photoactivatable green fluorescent protein. *Journal of the American Chemical Society*, *131*, 4176–4177.
Hirata, R., Hirakawa, K., Shimada, N., Watanabe, K., & Ohtsuki, T. (2021). Fluorescence lifetime probes for detection of RNA degradation. *Analyst*, *146*, 277–282.
Honda, Y., & Kirimura, K. (2013). Generation of circularly permuted fluorescent-protein-based indicators for in vitro and in vivo detection of citrate. *PLoS One*, *8*, e64597.
Hu, R., et al. (2014). Multicolor fluorescent biosensor for multiplexed detection of DNA. *Analytical Chemistry*, *86*, 5009–5016.
Huang, B., Bates, M., & Zhuang, X. (2009). Super-resolution fluorescence microscopy. *Annual Review of Biochemistry*, *78*, 993–1016.
Huang, B., Wang, W., Bates, M., & Zhuang, X. (2008). Three-dimensional super-resolution imaging by stochastic optical reconstruction microscopy. *Science*, *319*, 810–813.
Hung, Y. P., Albeck, J. G., Tantama, M., & Yellen, G. (2011). Imaging cytosolic NADH-NAD+ redox state with a genetically encoded fluorescent biosensor. *Cell Metabolism*, *14*, 545–554.
Imamura, H., et al. (2009). Visualization of ATP levels inside single living cells with fluorescence resonance energy transfer-based genetically encoded indicators. *Proceedings of the National Academy of Sciences*, *106*, 15651–15656.
Isoda, R., et al. (2021). Sensors for the quantification, localization and analysis of the dynamics of plant hormones. *The Plant Journal*, *105*, 542–557.
Ivanusic, D., Eschricht, M., & Denner, J. (2014). Investigation of membrane protein–protein interactions using correlative FRET-PLA. *BioTechniques*, *57*, 188–198.
Iyer, A., et al. (2021). Chemogenetic tags with probe exchange for live-cell fluorescence microscopy. *ACS Chemical Biology*. https://doi.org/10.1021/acschembio.1c00100.
James-Kracke, M. R. (1992). Quick and accurate method to convert BCECF fluorescence to pHi: Calibration in three different types of cell preparations. *Journal of Cellular Physiology*, *151*, 596–603.
Jepsen, M. D. E., et al. (2018). Development of a genetically encodable FRET system using fluorescent RNA aptamers. *Nature Communications*, *9*.
Jonkman, J., Brown, C. M., Wright, G. D., Anderson, K. I., & North, A. J. (2020). Tutorial: Guidance for quantitative confocal microscopy. *Nature Protocols*, *15*, 1585–1611.
Kamper, M., Ta, H., Jensen, N. A., Hell, S. W., & Jakobs, S. (2018). Near-infrared STED nanoscopy with an engineered bacterial phytochrome. *Nature Communications*, *9*, 4762.
Kano, K., & Fendler, J. H. (1978). Pyranine as a sensitive pH probe for liposome interiors and surfaces. pH gradients across phospholipid vesicles. *Biochimica et Biophysica Acta (BBA) - Biomembranes*, *509*, 289–299.
Kashirina, A. S., et al. (2020). Monitoring membrane viscosity in differentiating stem cells using BODIPY-based molecular rotors and FLIM. *Scientific Reports*, *10*, 14063.

Kaufmann, T., et al. (2020). Direct measurement of protein–protein interactions by FLIM-FRET at UV laser-induced DNA damage sites in living cells. *Nucleic Acids Research*, *48*(21), e122.
Kellenberger, C. A., Chen, C., Whiteley, A. T., Portnoy, D. A., & Hammond, M. C. (2015). RNA-based fluorescent biosensors for live cell imaging of second messenger cyclic di-AMP. *Journal of the American Chemical Society*, *137*, 6432–6435.
Kellenberger, C. A., Wilson, S. C., Sales-Lee, J., & Hammond, M. C. (2013). RNA-based fluorescent biosensors for live cell imaging of second messengers cyclic di-GMP and cyclic AMP-GMP. *Journal of the American Chemical Society*, *135*, 4906–4909.
Khater, I. M., Nabi, I. R., & Hamarneh, G. (2020). A review of super-resolution single-molecule localization microscopy cluster analysis and quantification methods. *Patterns*, *1*, 100038.
Kim, Y., et al. (2008). Efficient site-specific labeling of proteins via cysteines. *Bioconjugate Chemistry*, *19*, 786–791.
Kitajima, N., et al. (2020). Real-time in vivo imaging of extracellular ATP in the brain with a hybrid-type fluorescent sensor. *eLife*, *9*, e57544.
Knop, M. & Edgar, B. A. Tracking protein turnover and degradation by microscopy: Photo-switchable versus time-encoded fluorescent proteins. Open Biology 4, 140002.
Ko, W., Kim, S., & Lee, H. S. (2017). Engineering a periplasmic binding protein for amino acid sensors with improved binding properties. *Organic & Biomolecular Chemistry*, *15*, 8761–8769.
Kollenda, S., et al. (2020). A pH-sensitive fluorescent protein sensor to follow the pathway of calcium phosphate nanoparticles into cells. *Acta Biomaterialia*, *111*, 406–417.
Kostyuk, A. I., Demidovich, A. D., Kotova, D. A., Belousov, V. V., & Bilan, D. S. (2019). Circularly permuted fluorescent protein-based indicators: History, principles, and classification. *International Journal of Molecular Sciences*, *20*, 4200.
Kuimova, M. K. (2012). Mapping viscosity in cells using molecular rotors. *Physical Chemistry Chemical Physics*, *14*, 12671–12686.
Kundu, R., Chandra, A., & Datta, A. (2021). Fluorescent chemical tools for tracking anionic phospholipids. *Israel Journal of Chemistry*, *61*, 199–216.
Ladner, C. L., Turner, R. J., & Edwards, R. A. (2007). Development of indole chemistry to label tryptophan residues in protein for determination of tryptophan surface accessibility. *Protein Science: A Publication of the Protein Society*, *16*, 1204–1213.
Larda, S. T., Pichugin, D., & Prosser, R. S. (2015). Site-specific labeling of protein lysine residues and N-terminal amino groups with indoles and indole-derivatives. *Bioconjugate Chemistry*, *26*, 2376–2383.
Laxman, P., Ansari, S., Gaus, K., & Goyette, J. (2021). The benefits of unnatural amino acid incorporation as protein labels for single molecule localization microscopy. *Frontiers in Chemistry*, *9*, 161.
Lee, S.-C., et al. (2018). Fluorescent molecular rotors for viscosity sensors. *Chemistry - A European Journal*, *24*, 13706–13718.
Lerner, E., et al. (2021). FRET-based dynamic structural biology: Challenges, perspectives and an appeal for open-science practices. *eLife*, *10*, e60416.
Lichtman, J. W., & Conchello, J.-A. (2005). Fluorescence microscopy. *Nature Methods*, *2*, 910–919.
Lippincott-Schwartz, J., & Patterson, G. H. (2009). Photoactivatable fluorescent proteins for diffraction-limited and super-resolution imaging. *Trends in Cell Biology*, *19*, 555–565.
Liu, B., Poolman, B., & Boersma, A. J. (2017). Ionic strength sensing in living cells. *ACS Chemical Biology*, *12*, 2510–2514.
Liu, B., et al. (2017). Design and properties of genetically encoded probes for sensing macromolecular crowding. *Biophysical Journal*, *112*, 1929–1939.

Liu, B., et al. (2018). Influence of fluorescent protein maturation on FRET measurements in living cells. *ACS Sensors*, *3*, 1735–1742.
Liu, X., et al. (2020). Molecular mechanism of viscosity sensitivity in BODIPY rotors and application to motion-based fluorescent sensors. *ACS Sensors*, *5*, 731–739.
Liu, A., et al. (2021). pHmScarlet is a pH-sensitive red fluorescent protein to monitor exocytosis docking and fusion steps. *Nature Communications*, *12*, 1413.
Lukyanov, K. A., Chudakov, D. M., Lukyanov, S., & Verkhusha, V. V. (2005). Photoactivatable fluorescent proteins. *Nature Reviews. Molecular Cell Biology*, *6*, 885–890.
Ma, Y., Abbate, V., & Hider, R. C. (2015). Iron-sensitive fluorescent probes: Monitoring intracellular iron pools. *Metallomics*, *7*, 212–222.
Ma, Y., Sun, Q., & Smith, S. C. (2017). The mechanism of oxidation in chromophore maturation of wild-type green fluorescent protein: A theoretical study. *Physical Chemistry Chemical Physics*, *19*, 12942–12952.
Mahon, M. J. (2011). pHluorin2: An enhanced, ratiometric, pH-sensitive green florescent protein. *Advances in Bioscience and Biotechnology*, *2*, 132–137.
Maksimov, E. G., et al. (2019). A genetically encoded fluorescent temperature sensor derived from the photoactive Orange Carotenoid Protein. *Scientific Reports*, *9*, 8937.
Mao, S.-Y., & Mullins, J. M. (2010). Conjugation of fluorochromes to antibodies. In C. Oliver, & M. C. Jamur (Eds.), *Immunocytochemical Methods and Protocols* (pp. 43–48). Humana Press. https://doi.org/10.1007/978-1-59745-324-0_6.
Margineanu, A., et al. (2016). Screening for protein-protein interactions using Förster resonance energy transfer (FRET) and fluorescence lifetime imaging microscopy (FLIM). *Scientific Reports*, *6*, 28186.
Marshall, A. (2000). Red fluorescent protein structure. *Nature Biotechnology*, *18*, 1231.
McNamara, K. P., & Rosenzweig, Z. (1998). Dye-encapsulating liposomes as fluorescence-based oxygen nanosensors. *Analytical Chemistry*, *70*, 4853–4859.
Meier, S. D., Kovalchuk, Y., & Rose, C. R. (2006). Properties of the new fluorescent Na+ indicator CoroNa Green: Comparison with SBFI and confocal Na+ imaging. *Journal of Neuroscience Methods*, *155*, 251–259.
Miesenböck, G., De Angelis, D. A., & Rothman, J. E. (1998). Visualizing secretion and synaptic transmission with pH-sensitive green fluorescent proteins. *Nature*, *394*, 192–195.
Mika, J. T., Krasnikov, V., van den Bogaart, G., de Haan, F., & Poolman, B. (2011). Evaluation of pulsed-FRAP and conventional-FRAP for determination of protein mobility in prokaryotic cells. *PLoS One*, *6*, e25664.
Minta, A., & Tsien, R. Y. (1989). Fluorescent indicators for cytosolic sodium*. *The Journal of Biological Chemistry*, *264*, 19449–19457.
Mirabello, V., Cortezon-Tamarit, F., & Pascu, S. I. (2018). Oxygen sensing, hypoxia tracing and in vivo imaging with functional metalloprobes for the early detection of non-communicable diseases. *Frontiers in Chemistry*, *6*, 27.
Miyawaki, A., et al. (1997). Fluorescent indicators for Ca2+ based on green fluorescent proteins and calmodulin. *Nature*, *388*, 882–887.
Mizuno, H., et al. (2003). Photo-induced peptide cleavage in the green-to-red conversion of a fluorescent protein. *Molecular Cell*, *12*, 1051–1058.
Molenaar, C., Abdulle, A., Gena, A., Tanke, H. J., & Dirks, R. W. (2004). Poly(A)+ RNAs roam the cell nucleus and pass through speckle domains in transcriptionally active and inactive cells. *The Journal of Cell Biology*, *165*, 191–202.
Molenaar, C., Wiesmeijer, K., Verwoerd, N. P., Khazen, S., Eils, R., Tanke, H. J., et al. (2003). Visualizing telomere dynamics in living mammalian cells using PNA probes. *The EMBO Journal*, *22*, 6631–6641.
Nadler, D. C., Morgan, S.-A., Flamholz, A., Kortright, K. E., & Savage, D. F. (2016). Rapid construction of metabolite biosensors using domain-insertion profiling. *Nature Communications*, *7*, 12266.

Nagai, T., Sawano, A., Park, E. S., & Miyawaki, A. (2001). Circularly permuted green fluorescent proteins engineered to sense Ca2+. *Proceedings of the National Academy of Sciences*, *98*, 3197–3202.

Naganathan, A. N., & Muñoz, V. (2005). Scaling of folding times with protein size. *Journal of the American Chemical Society*, *127*, 480–481.

Nasu, Y., Shen, Y., Kramer, L., & Campbell, R. E. (2021). Structure- and mechanism-guided design of single fluorescent protein-based biosensors. *Nature Chemical Biology*, *17*, 509–518.

Nienhaus, K., & Nienhaus, G. U. (2017). Fluorescent proteins for super-resolution microscopy. *Biophysical Journal*, *112*(453a).

Okabe, K., et al. (2012). Intracellular temperature mapping with a fluorescent polymeric thermometer and fluorescence lifetime imaging microscopy. *Nature Communications*, *3*, 705.

Okuda, M., Fourmy, D., & Yoshizawa, S. (2017). Use of baby spinach and broccoli for imaging of structured cellular RNAs. *Nucleic Acids Research*, *45*, 1404–1415.

Okumoto, S., Jones, A., & Frommer, W. B. (2012). Quantitative imaging with fluorescent biosensors. *Annual Review of Plant Biology*, *63*, 663–706.

Oliveira, E., et al. (2018). Green and red fluorescent dyes for translational applications in imaging and sensing analytes: A dual-color flag. *ChemistryOpen*, *7*, 9–52.

Otten, J., et al. (2019). A FRET-based biosensor for the quantification of glucose in culture supernatants of mL scale microbial cultivations. *Microbial Cell Factories*, *18*, 143.

Ouellet, J. (2016). RNA fluorescence with light-up aptamers. *Frontiers in Chemistry*, *4*, 29.

Ozkan, P., & Mutharasan, R. (2002). A rapid method for measuring intracellular pH using BCECF-AM. *Biochimica et Biophysica Acta*, *1572*, 143–148.

Paredes, R. M., Etzler, J. C., Watts, L. T., & Lechleiter, J. D. (2008). Chemical calcium indicators. *Methods San Diego Calif*, *46*, 143–151.

Park, S., Kang, S., & Yoon, T.-S. (2016). Crystal structure of the cyan fluorescent protein Cerulean-S175G. *Acta Crystallographica Section F: Structural Biology Communications*, *72*, 516–522.

Patel, H., Tscheka, C., & Heerklotz, H. (2009). Characterizing vesicle leakage by fluorescence lifetime measurements. *Soft Matter*, *5*, 2849–2851.

Pédelacq, J.-D., Cabantous, S., Tran, T., Terwilliger, T. C., & Waldo, G. S. (2006). Engineering and characterization of a superfolder green fluorescent protein. *Nature Biotechnology*, *24*, 79–88.

Periasamy, A., Mazumder, N., Sun, Y., Christopher, K. G., & Day, R. N. (2015). FRET microscopy: Basics, issues and advantages of FLIM-FRET imaging. In W. Becker (Ed.), *Advanced time-correlated single photon counting applications* (pp. 249–276). Springer International Publishing. https://doi.org/10.1007/978-3-319-14929-5_7.

Pettersen, E. F., et al. (2004). UCSF Chimera—A visualization system for exploratory research and analysis. *Journal of Computational Chemistry*, *25*, 1605–1612.

Phillips, D., Drake, R. C., O'Connor, D. V., & Christensen, R. L. (1985). Time correlated single-photon counting (Tcspc) using laser excitation. *Instrumentation Science and Technology*, *14*, 267–292.

Pincet, F., et al. (2016). FRAP to characterize molecular diffusion and interaction in various membrane environments. *PLoS One*, *11*, e0158457.

Plamont, M.-A., et al. (2016). Small fluorescence-activating and absorption-shifting tag for tunable protein imaging in vivo. *Proceedings of the National Academy of Sciences*, *113*, 497–502.

Pletnev, S., Subach, F. V., Dauter, Z., Wlodawer, A., & Verkhusha, V. V. (2010). Understanding blue-to-red conversion in monomeric fluorescent timers and hydrolytic degradation of their chromophores. *Journal of the American Chemical Society*, *132*, 2243–2253.

Ploetz, E. *et al*. Structural and biophysical characterization of the tandem substrate-binding domains of the ABC importer GlnPQ. Open Biology 11, 200406.
Politz, J. C., Taneja, K. L., & Singer, R. H. (1995). Characterization of hybridization between synthetic oligodeoxynuclotides and RNA in living cells. *Nucleic Acids Research*, *23*, 4946–4953.
Pols, T., et al. (2019). A synthetic metabolic network for physicochemical homeostasis. *Nature Communications*, *10*, 4239.
Pothoulakis, G., Ceroni, F., Reeve, B., & Ellis, T. (2014). The spinach RNA aptamer as a characterization tool for synthetic biology. *ACS Synthetic Biology*, *3*, 182–187.
Poudel, C., Mela, I., & Kaminski, C. F. (2020). High-throughput, multi-parametric, and correlative fluorescence lifetime imaging. *Methods and Applications in Fluorescence*, *8*, 024005.
Prasher, D. C., Eckenrode, V. K., Ward, W. W., Prendergast, F. G., & Cormier, M. J. (1992). Primary structure of the Aequorea victoria green-fluorescent protein. *Gene*, *111*, 229–233.
Qu, D., et al. (2011). 5-Ethynyl-2′-deoxycytidine as a new agent for DNA labeling: Detection of proliferating cells. *Analytical Biochemistry*, *417*, 112–121.
Reid, B. G., & Flynn, G. C. (1997). Chromophore formation in green fluorescent protein. *Biochemistry*, *36*, 6786–6791.
Remington, S. J. (2006). Fluorescent proteins: Maturation, photochemistry and photophysics. *Current Opinion in Structural Biology*, *16*, 714–721.
Renz, M. (2013). Fluorescence microscopy—A historical and technical perspective. *Cytometry. Part A*, *83*, 767–779.
Roberts, T. M., et al. (2016). Identification and Characterisation of a pH-stable GFP. *Scientific Reports*, *6*, 28166.
Rodriguez, E. A., et al. (2017). The growing and glowing toolbox of fluorescent and photoactive proteins. *Trends in Biochemical Sciences*, *42*, 111–129.
Roldán-Salgado, A., Sánchez-Barreto, C., & Gaytán, P. (2016). LanFP10-A, first functional fluorescent protein whose chromophore contains the elusive mutation G67A. *Gene*, *592*, 281–290.
Romei, M. G., & Boxer, S. G. (2019). Split green fluorescent proteins: Scope, limitations, and outlook. *Annual Review of Biophysics*, *48*, 19–44.
Rust, M. J., Bates, M., & Zhuang, X. (2006). Sub-diffraction-limit imaging by stochastic optical reconstruction microscopy (STORM). *Nature Methods*, *3*, 793–796.
Sadoine, M., Reger, M., Wong, K. M., & Frommer, W. B. (2021). Affinity series of genetically encoded Förster resonance energy-transfer sensors for sucrose. *ACS Sensors*, *6*, 1779–1784.
Salic, A., & Mitchison, T. J. (2008). A chemical method for fast and sensitive detection of DNA synthesis in vivo. *Proceedings of the National Academy of Sciences*, *105*, 2415–2420.
Saxon, E., Armstrong, J. I., & Bertozzi, C. R. (2000). A "traceless" Staudinger ligation for the chemoselective synthesis of amide bonds. *Organic Letters*, *2*, 2141–2143.
Schavemaker, P. E., Śmigiel, W. M., & Poolman, B. (2017). Ribosome surface properties may impose limits on the nature of the cytoplasmic proteome. *eLife*, *6*, e30084.
Scheepers, G. H., Nijeholt, J. A. L. A., & Poolman, B. (2016). An updated structural classification of substrate-binding proteins. *FEBS Letters*, *590*, 4393–4401.
Shaner, N. C., et al. (2013). A bright monomeric green fluorescent protein derived from Branchiostoma lanceolatum. *Nature Methods*, *10*, 407–409.
Shcherbakova, D. M., Sengupta, P., Lippincott-Schwartz, J., & Verkhusha, V. V. (2014). Photocontrollable fluorescent proteins for superresolution imaging. *Annual Review of Biophysics*, *43*, 303–329.
Shen, Y., Rosendale, M., Campbell, R. E., & Perrais, D. (2014). pHuji, a pH-sensitive red fluorescent protein for imaging of exo- and endocytosis. *The Journal of Cell Biology*, *207*, 419–432.

Shen, Y., et al. (2019). Genetically encoded fluorescent indicators for imaging intracellular potassium ion concentration. *Communications Biology*, *2*, 1–10.
Shi, J., Heegaard, C. W., Rasmussen, J. T., & Gilbert, G. E. (2004). Lactadherin binds selectively to membranes containing phosphatidyl-l-serine and increased curvature. *Biochimica et Biophysica Acta (BBA) - Biomembranes*, *1667*, 82–90.
Shimomura, O., Johnson, F. H., & Saiga, Y. (1962). Extraction, purification and properties of aequorin, a bioluminescent protein from the luminous hydromedusan, aequorea. *Journal of Cellular and Comparative Physiology*, *59*, 223–239.
Shinoda, H., et al. (2018). Acid-Tolerant Monomeric GFP from Olindias formosa. *Cell Chemical Biology*, *25*, 330–338. e7.
Shrestha, D., Jenei, A., Nagy, P., Vereb, G., & Szöllősi, J. (2015). Understanding FRET as a research tool for cellular studies. *International Journal of Molecular Sciences*, *16*, 6718–6756.
Sims, P. J., Waggoner, A. S., Wang, C.-H., & Hoffman, J. F. (1974). Mechanism by which cyanine dyes measure membrane potential in red blood cells and phosphatidylcholine vesicles. *Biochemistry*, *13*, 3315–3330.
Sniegowski, J. A., Phail, M. E., & Wachter, R. M. (2005). Maturation efficiency, trypsin sensitivity, and optical properties of Arg96, Glu222, and Gly67 variants of green fluorescent protein. *Biochemical and Biophysical Research Communications*, *332*, 657–663.
Solenov, E., Watanabe, H., Manley, G. T., & Verkman, A. S. (2004). Sevenfold-reduced osmotic water permeability in primary astrocyte cultures from AQP-4-deficient mice, measured by a fluorescence quenching method. *American Journal of Physiology. Cell Physiology*, *286*, C426–C432.
Somerville, G. A., & Proctor, R. A. (2009). At the crossroads of bacterial metabolism and virulence factor synthesis in Staphylococci. *Microbiology and Molecular Biology Reviews*, *73*, 233–248.
Specht, E. A., Braselmann, E., & Palmer, A. E. (2017). A critical and comparative review of fluorescent tools for live-cell imaging. *Annual Review of Physiology*, *79*, 93–117.
Spötl, L., Sarti, A., Dierich, M. P., & Möst, J. (1995). Cell membrane labeling with fluorescent dyes for the demonstration of cytokine-induced fusion between monocytes and tumor cells. *Cytometry*, *21*, 160–169.
Stepanenko, O. V., et al. (2011). Modern fluorescent proteins: From chromophore formation to novel intracellular applications. *BioTechniques*, *51*, 313–327.
Strack, R. (2021). Organic dyes for live imaging. *Nature Methods*, *18*, 30.
Strack, R. L., Strongin, D. E., Mets, L., Glick, B. S., & Keenan, R. J. (2010). Chromophore formation in DsRed occurs by a branched pathway. *Journal of the American Chemical Society*, *132*, 8496–8505.
Suhling, K., Davis, D. M., & Phillips, D. (2002). The influence of solvent viscosity on the fluorescence decay and time-resolved anisotropy of green fluorescent protein. *Journal of Fluorescence*, *12*, 91–95.
Suhling, K., et al. (2002). Imaging the environment of green fluorescent protein. *Biophysical Journal*, *83*, 3589–3595.
Sukhorukov, V. M., et al. (2010). Determination of protein mobility in mitochondrial membranes of living cells. *Biochimica et Biophysica Acta (BBA) - Biomembranes*, *1798*, 2022–2032.
Sun, Y., Hays, N. M., Periasamy, A., Davidson, M. W., & Day, R. N. (2012). Chapter nineteen—Monitoring protein interactions in living cells with fluorescence lifetime imaging microscopy. In P. M. Conn (Ed.), *504. Methods in Enzymology* (pp. 371–391). Academic Press.
Szmacinski, H., & Lakowicz, J. R. (1997). Sodium green as a potential probe for intracellular sodium imaging based on fluorescence lifetime. *Analytical Biochemistry*, *250*, 131–138.
Takaoka, Y., Ojida, A., & Hamachi, I. (2013). Protein organic chemistry and applications for labeling and engineering in live-cell systems. *Angewandte Chemie, International Edition*, *52*, 4088–4106.

Tantama, M., Hung, Y. P., & Yellen, G. (2011). Imaging intracellular pH in live cells with a genetically encoded red fluorescent protein sensor. *Journal of the American Chemical Society*, *133*, 10034–10037.

Tantama, M., Martínez-François, J. R., Mongeon, R., & Yellen, G. (2013). Imaging energy status in live cells with a fluorescent biosensor of the intracellular ATP-to-ADP ratio. *Nature Communications*, *4*, 2550.

Tao, R., et al. (2017). Genetically encoded fluorescent sensors reveal dynamic regulation of NADPH metabolism. *Nature Methods*, *14*, 720–728.

Tebo, A. G., et al. (2018). Circularly permuted fluorogenic proteins for the design of modular biosensors. *ACS Chemical Biology*, *13*, 2392–2397.

Tebo, A. G., et al. (2021). Orthogonal fluorescent chemogenetic reporters for multicolor imaging. *Nature Chemical Biology*, *17*, 30–38.

Tokunaga, M., Imamoto, N., & Sakata-Sogawa, K. (2008). Highly inclined thin illumination enables clear single-molecule imaging in cells. *Nature Methods*, *5*, 159–161.

Tomosugi, W., et al. (2009). An ultramarine fluorescent protein with increased photostability and pH insensitivity. *Nature Methods*, *6*, 351–353.

Topell, S., Hennecke, J., & Glockshuber, R. (1999). Circularly permuted variants of the green fluorescent protein. *FEBS Letters*, *457*, 283–289.

Tramier, M., & Coppey-Moisan, M. (2008). Fluorescence anisotropy imaging microscopy for homo-FRET in living cells. In *85. Methods in Cell Biology* (pp. 395–414). Academic Press.

Trauth, J., et al. (2020). Strategies to investigate protein turnover with fluorescent protein reporters in eukaryotic organisms. *AIMS Biophysics*, 7, 90–118.

Tregidgo, C. L., Levitt, J. A., & Suhling, K. (2008). Effect of refractive index on the fluorescence lifetime of green fluorescent protein. *Journal of Biomedical Optics*, *13*, 031218.

Tsien, R. Y. (1998). The green fluorescent protein. *Annual Review of Biochemistry*, *67*, 509–544.

Vaidyanathan, P., et al. (2021). Algorithms for the selection of fluorescent reporters. *Communications Biology*, *4*, 1–8.

van Berkel, S. S., van Eldijk, M. B., & van Hest, J. C. M. (2011). Staudinger ligation as a method for bioconjugation. *Angewandte Chemie, International Edition*, *50*, 8806–8827.

van den Berg, J., Boersma, A. J., & Poolman, B. (2017). Microorganisms maintain crowding homeostasis. *Nature Reviews. Microbiology*, *15*, 309–318.

van der Heide, T., Stuart, M. C., & Poolman, B. (2001). On the osmotic signal and osmosensing mechanism of an ABC transport system for glycine betaine. *The EMBO Journal*, *20*, 7022–7032.

van der Meer, B. W. (2002). Kappa-squared: From nuisance to new sense. *Reviews in Molecular Biotechnology*, *82*, 181–196.

Várnai, P., & Balla, T. (2006). Live cell imaging of phosphoinositide dynamics with fluorescent protein domains. *Biochimica et Biophysica Acta (BBA) - Molecular and Cell Biology of Lipids*, *1761*, 957–967.

Verkhusha, V. V., Chudakov, D. M., Gurskaya, N. G., Lukyanov, S., & Lukyanov, K. A. (2004). Common pathway for the red chromophore formation in fluorescent proteins and chromoproteins. *Chemistry & Biology*, *11*, 845–854.

Wachter, R. M., Elsliger, M.-A., Kallio, K., Hanson, G. T., & Remington, S. J. (1998). Structural basis of spectral shifts in the yellow-emission variants of green fluorescent protein. *Structure*, *6*, 1267–1277.

Wachter, R. M., Watkins, J. L., & Kim, H. (2010). Mechanistic diversity of red fluorescence acquisition by GFP-like proteins. *Biochemistry*, *49*, 7417–7427.

Wakelam, M. J. O. (2014). The uses and limitations of the analysis of cellular phosphoinositides by lipidomic and imaging methodologies. *Biochimica et Biophysica Acta (BBA) - Molecular and Cell Biology of Lipids*, *1841*, 1102–1107.

Wang, S., Moffitt, J. R., Dempsey, G. T., Xie, X. S., & Zhuang, X. (2014). Characterization and development of photoactivatable fluorescent proteins for single-molecule–based superresolution imaging. *Proceedings of the National Academy of Sciences*, *111*, 8452–8457.

Wang, L., et al. (2016). A multisite-binding switchable fluorescent probe for monitoring mitochondrial ATP level fluctuation in live cells. *Angewandte Chemie, International Edition*, *55*, 1773–1776.

Wang, X. C., Wilson, S. C., & Hammond, M. C. (2016). Next-generation RNA-based fluorescent biosensors enable anaerobic detection of cyclic di-GMP. *Nucleic Acids Research*, *44*(17), e139.

Ward, W. W., Prentice, H. J., Roth, A. F., Cody, C. W., & Reeves, S. C. (1982). Spectral perturbations of the aequorea green-fluorescent protein. *Photochemistry and Photobiology*, *35*, 803–808.

Wazawa, T., et al. (2021). A photoswitchable fluorescent protein for hours-time-lapse and sub-second-resolved super-resolution imaging. *Microscopy*, *70*, 340–352.

Westerhof, T. M., Li, G.-P., Bachman, M., & Nelson, E. L. (2016). Multicolor immunofluorescent imaging of complex cellular mixtures on micropallet arrays enables the identification of single cells of defined phenotype. *Advanced Healthcare Materials*, *5*, 767–771.

Xiang, L., Chen, K., Yan, R., Li, W., & Xu, K. (2020). Single-molecule displacement mapping unveils nanoscale heterogeneities in intracellular diffusivity. *Nature Methods*, *17*, 524–530.

Yaginuma, H., et al. (2014). Diversity in ATP concentrations in a single bacterial cell population revealed by quantitative single-cell imaging. *Scientific Reports*, *4*, 6522.

Yang, F., Moss, L. G., & Phillips, G. N. (1996). The molecular structure of green fluorescent protein. *Nature Biotechnology*, *14*, 1246–1251.

Zhang, G., Gurtu, V., & Kain, S. R. (1996). An enhanced green fluorescent protein allows sensitive detection of gene transfer in mammalian cells. *Biochemical and Biophysical Research Communications*, *227*, 707–711.

Zhang, J., et al. (2015). Tandem spinach array for mRNA imaging in living bacterial cells. *Scientific Reports*, *5*, 17295.

Zhao, Y., et al. (2011). Genetically encoded fluorescent sensors for intracellular NADH detection. *Cell Metabolism*, *14*, 555–566.

Zhao, Y., et al. (2015). SoNar, a highly responsive NAD+/NADH sensor, allows high-throughput metabolic screening of anti-tumor agents. *Cell Metabolism*, *21*, 777–789.

Zhou, X. X., & Lin, M. Z. (2013). Photoswitchable fluorescent proteins: Ten years of colorful chemistry and exciting applications. *Current Opinion in Chemical Biology*, *17*, 682–690.